Photoprotons from Oxygen, Fluorine, Neon, and Other Light Elements*

W. R. DODGE† AND W. C. BARBER
High-Energy Physics Laboratory, Stanford University, Stanford, California

(Received April 2, 1962)

The (γ,p) reaction in O, F, Ne, and C has been studied with electrons of energies up to 36 MeV. Survey studies were made of the Al, Ar, and B (γ,p) energy spectra. The reactions were initiated by electrons, and not real photons, but it has been theoretically predicted and received partial experimental verification that there is a one-to-one correspondence between electron- and photon-induced reactions, and that one can assume, when analyzing electron-production yields, that the electron has associated with it a virtual-photon spectrum, similar to the real-photon bremsstrahlung spectrum. The virtual and bremsstrahlung spectra differ, however, in that the virtual-photon spectrum depends on the multipolarity of the induced transition and the angle between the incident electron beam and the emitted disintegration product, while the bremsstrahlung spectrum does not. The electron production yields were analyzed with the use of the $E1$ virtual-photon spectrum to obtain $\sigma(\gamma,p)$. The proton yields and corresponding cross section of O, F, and Ne contain more than two peaks or resonances. Neon exhibits the most interesting spectrum. It has a series of well-resolved, evenly spaced peaks whose envelope has the usual giant-resonance shape. The peaks occur at laboratory proton energies of 3.20, 3.70, 4.58, 5.80, 6.65, 7.75, 8.65, 9.40, and 11.40 MeV. The final-state properties of the Ne protons from 4 to 10 MeV and the O protons from 9.2 to 12.4 MeV were determined to within 20% by excitation experiments. Angular distribution measurements over a considerable region of the giant resonances are presented for O, F, Ne, and C.

I. INTRODUCTION

IT is generally conceded that the mechanism of photonuclear reactions is essentially understood, yet a number of important facets of these reactions still await experimental confirmation and quantitative theoretical explanation. Among the unexplained facets is the "contentious" subject[1] of gross structure in the giant resonance in light nuclei, as conjectured from the γ-nucleon cross sections. This subject is nontrivial, since the occurrence of gross structure other than that attributable to a deformation of the nuclear shape from sphericity, as evidenced by large quadrupole moments, is embarrassing to the collective models of the nuclear photoeffect, while the independent-particle models contain an inherent mechanism for the production of structure.[2] While, in general, the two models have mutually exclusive domains of validity, regions do exist where both models claim applicability. As Spicer[3] has pointed out, since the properties of the low-lying states of elements in the region of $9<Z<30$ are successfully described by the collective or strong interaction models, the Danos-Okamoto long-range correlation model[4] of the photonuclear effect must be applicable to these elements. If the collective-model description is correct in this region, the giant resonance should be split into two peaks occurring at photon energies ω_a and ω_b whose ratio is given by $\omega_a/\omega_b=0.911(a/b)+0.089$, where the ratio a/b (a and b are the lengths of the semimajor and semiminor axes of the assumed spheroidally shaped nucleus) can be determined from the intrinsic quadrupole moment. In particular, using values for the intrinsic quadrupole moments derived from low-lying $E2$ transitions,[5] the collective model predicts ω_a/ω_b values of 1.3 and 1.4 for F and Ne, respectively; hence, the predicted giant-resonance splitting should be easily resolved. On the other hand, recent theoretical studies show that Wilkinson's theory[6] of the photonuclear effect with detailed shell-model initial and excited states[7,8] can well parody the gross structure previously seen in the O $\sigma(\gamma,p)$. Furthermore, although detailed photonuclear calculations have not been made for F and Ne, the excited states of F^{19} have been calculated with the shell model using configuration mixing.[9] These elements should clearly be within the domain of the shell model.[10] Thus, both models claim to be applicable to the photonuclear effect in F and Ne. Therefore, the occurrence of more than two or, if the improbable assumption of nonaxial nuclear symmetry[11] is made, three relatively large peaks in $\sigma(\gamma,p)$ would confirm the independent-particle-model description of the nuclear photoeffect while providing a severe censure of the collective-model description. Noncommittal results might give some insight into the coupling mechanism between the single-particle states and collective-model states in the nuclear-model transition region. However, except for the O $\sigma(\gamma,p)$, experimental evi-

* This work was supported by the joint program of the Office of Naval Research, the U. S. Atomic Energy Commission, and the Air Force Office of Scientific Research.

† Now at the High-Energy Radiation Section of the National Bureau of Standards, Washington 25, D. C.

[1] D. H. Wilkinson, Ann. Rev. Nuclear Sci. **9**, 1 (1959).
[2] D. H. Wilkinson, reference 1, p. 18.
[3] B. M. Spicer, Australian J. Phys. **11**, 490 (1958)
[4] M. Danos, Nuclear Phys. **5** 23 (1958).
[5] G. Rakavy, Nuclear Phys. **4**, 375 (1957).
[6] D. H. Wilkinson, in *Proceedings of the 1954 Glasgow Conference on Nuclear and Meson Physics* (Pergamon Press, New York, 1955), pp. 161–167.
[7] J. P. Elliot and B. H. Flowers, Proc. Roy. Soc. (London) **A242**, 57 (1957).
[8] G. E. Brown, L. Castillejo, and J. A. Evans, in *Contributions to the Karlsruhe Conference, 1960* (Erstes Physikalisches Institut der Universität Heidelberg, Heidelberg, 1961), p. B4.
[9] B. H. Flowers and J. P. Elliot, Proc. Roy. Soc. (London) **A229**, 537 (1955).
[10] D. H. Wilkinson, Physica **22**, 1149A (1956); and Phil. Mag. **3**, 567 (1958).
[11] A. S. Davydov and G. F. Filippov, Nuclear Phys. **8**, 237 (1955); **12**, 58 (1959).

dence for the gross (γ,p) energy structure has been statistically inconclusive.[12–15]

Consequently, a search for (γ,p) energy structure with which the predictions of the collective and independent particle models could be compared was made in O, F, and Ne. In addition, survey searches were made for (γ,p) energy structure in Ar and B, and a C energy spectrum, needed in the CF_2 target F experiments for C background subtraction, was obtained. Angular distributions of the protons from the prominent peaks in O, F, Ne, and C were measured. The relationship between photon and proton energy was determined for the major O and Ne peaks by excitation of the protons as a function of electron energy. All target elements contained the naturally occurring ratios of isotopes.

In these experiments the direct effect of the electron's transition electromagnetic field produced the reaction and not real photons. However, a direct correspondence between electron- and photon-induced reactions has been predicted by calculations that employ the Møller potential[16,17] to describe the electron's transition electromagnetic field. According to virtual-photon theory, the direct effect of the electron's transition field may be considered as spectra of virtual photons which depend on the multipolarity of the induced reaction. The electron-production yields may be analyzed with these virtual-photon spectra in analogy to the analysis of photoproduction yields with a real bremsstrahlung spectrum. The virtual-photon hypothesis and spectra have received partial experimental confirmation.[18,19] Therefore, we describe the electron-production process as a (γ,p) reaction, even though the square of the four-vector momentum transferred to the nucleus may be different than zero, as in the real-photon case. Furthermore, since the three-momentum transfer may be in other than incident-beam directions, although nearly forward directions predominate, the virtual-photon spectra are expected to have a slight dependence on the angle between the emitted disintegration product and the primary electron beam, and consequently, electron-induced angular disintegrations are expected to be slightly more isotropic than real-photon-induced reactions. This effect for $E1$ transitions has been examined theoretically by Bosco and Fubini.[20] They assume explicitly the classical $E1$ approximation ($kR \ll 1$, where k is subsequently defined and R is the radius of the interaction region) and implicitly the equality of the matrix elements of the current operator between initial nuclear and final nuclear-nucleon states which are perpendicular and parallel to the three-vector momentum transfer. Their result, which contained several printing errors, was not integrated over the scattered electron directions. They showed essentially that the $E1$ differential electron-disintegration cross section is given by

$$\frac{d^2\sigma}{d\Omega_q d\Omega_{e'}}=\frac{2\pi}{v_e}\rho_{e'}\rho_q\left[\tfrac{1}{2}\alpha(E)N_{ii}+\frac{\beta(E)}{q^2}N_{ij}q_iq_j\right], \quad (1)$$

if the $E1$ photodisintegration cross section is given by

$$d\sigma_{ph}/d\Omega_q=(2\pi/c)\rho_q[\alpha(E)+\beta(E)\sin^2\theta_q], \quad (2)$$

where

$$N_{ij}=\frac{e^2}{2m^2(k_0^2-\mathbf{k}^2)^2}\left\{2p_ip_j+\tfrac{1}{2}(\mathbf{k}^2-k_0^2)\delta_{ij}+(k_ik_j-p_ik_j-p_jk_i)\left(1-\frac{\mathbf{k}^2}{k_0^2}+\frac{2\mathbf{p}\cdot\mathbf{k}}{k_0^2}\right)+\frac{k_ik_j}{k_0^2}[2(\mathbf{p}\cdot\mathbf{k})^2-2\mathbf{k}^2(\mathbf{p}\cdot\mathbf{k})+\tfrac{1}{2}(\mathbf{k}^2-k_0^2)\mathbf{k}^2]\right\},$$

and θ_q is the angle between the real-photon direction and the relative momentum of the emitted particle $\mathbf{q}$. This is equivalent to

$$\frac{d^2\sigma}{d\Omega_q d\Omega_{e'}}=\pi\frac{\rho_{e'}\rho_q}{v_e}\frac{e^2}{m^2k_0^2}\left\{\tfrac{1}{2}\alpha(E)\left[-\tfrac{1}{2}-\frac{\omega^2+\omega'^2}{k_0^2-\mathbf{k}^2}-\frac{2m^2k_0^2}{(k_0^2-\mathbf{k}^2)^2}\right]+\frac{\beta(E)}{q^2}\left[\frac{2[(\omega'\mathbf{p}-\omega\mathbf{p}')\cdot\mathbf{q}]^2}{(k_0^2-\mathbf{k}^2)^2}+\frac{1}{2}\frac{(\mathbf{k}\cdot\mathbf{q})^2-k_0^2\mathbf{q}^2}{(k_0^2-\mathbf{k}^2)}\right]\right\}, \quad (3)$$

where $k_0=\omega-\omega'$ is the energy and $\mathbf{k}=\mathbf{p}-\mathbf{p}'$ is the momentum transferred to the disintegrating system; the unprimed quantities refer to initial- and the primed quantities to final-state electron variables. Upon integration over scattered-electron directions, we obtain

$$\frac{d\sigma}{d\Omega_q}=\pi^2\frac{e^2}{m^2k_0^2}\frac{\rho_{e'}\rho_q}{v_e}\left[\left(\frac{\omega^2+\omega'^2}{\omega\omega'}\lambda-2\right)\alpha(E)+\frac{\omega'}{\omega}\beta(E)+\left(\frac{\omega^2+\omega'^2}{\omega\omega'}\lambda-2-\frac{3}{2}\frac{\omega'}{\omega}\right)\beta(E)\sin^2\theta_q\right], \quad (4)$$

[12] W. E. Stephens, A. K. Mann, B. J. Patton, and E. J. Winhold, Phys. Rev. 98, 839 (1955).
[13] A. E. Sven Johansson and B. Forkman, Arkiv Fysik **12**, 359 (1957).
[14] U. Hegel and E. Finckh, Z. Physik **162**, 142 (1961).
[15] G. C. Thomas and N. W. Tanner, in *Contributions to the Karlsruhe Conference, 1960* (Erstes Physikalisches Institut der Universität Heidelberg, Heidelberg, 1961), p. P6 (post deadline paper).
[16] E. Guth and C. J. Mullin, Phys. Rev. **76**, 234 (1949).
[17] R. H. Dalitz and D. R. Yennie, Phys. Rev. **105**, 1598 (1957); and elsewhere in the same article.
[18] K. L. Brown and R. Wilson, Phys. Rev. **93**, 443 (1954).
[19] R. L. Hines, Phys. Rev. **105**, 1534 (1957).
[20] B. Bosco and S. Fubini, Nuovo cimento **9**, 350 (1958).

where

$$\lambda=\ln[(\omega\omega'+pp'-m^2)/m(\omega-\omega')].$$

II. EXPERIMENTAL APPARATUS AND METHODS

The major components of the experimental apparatus, the 49-MeV Stanford Mark II Linear Accelerator, the electron momentum-analyzing system,[21] and the 120° double-focusing, proton momentum-analyzing magnet, were the same as used in previous Stanford photoproton experiments.[22] However, the following modifications and innovations were made which resulted in substantial improvement of the proton-energy resolution and of the general experimental performance. A ported scattering chamber, designed to allow proton angular distributions to be measured in the angular range of 20 to 160°, reduced the matter the electron beam traversed before the target to 0.00075 in. of Al, which constituted the three-foil, secondary-emission electron-beam-current monitor (SEM)[23] and a 0.001-in. Al window between the accelerator and scattering-chamber vacuum systems. A new counter system which consisted of eight channels, each with an RCA 6810 photomultiplier tube with a vacuum seal at the projecting metal ring on the tube base, was constructed. This system permitted the photocathode of the PMT and the 1.125×2.00×0.010-in. Pilot B scintillators,[24] on which were evaporated approximately 10^{-5} in. of Al for optical isolation of the counters, to be in the spectrometer vacuum system. The effective spectrometer resolution was increased by decreasing the scintillator width in the direction of momentum dispersion to 1.125 in. and by a feature of the counter system which allowed independent and accurate positioning of each counter in the spectrometer focal surface. The outputs of the PMT's were fed directly to fast integral discriminators of the Moody[25] type. The resolving time for the entire counter system was less than 30 nsec, and this greatly improved resolving time eliminated, to a large degree, background from pile-up of small electron-induced pulses, and allowed the maximum electron-beam current to be used, thus improving the counting-rate statistics. Since the scintillators contained hydrogen, additional neutron shielding was necessary to eliminate the possibility of

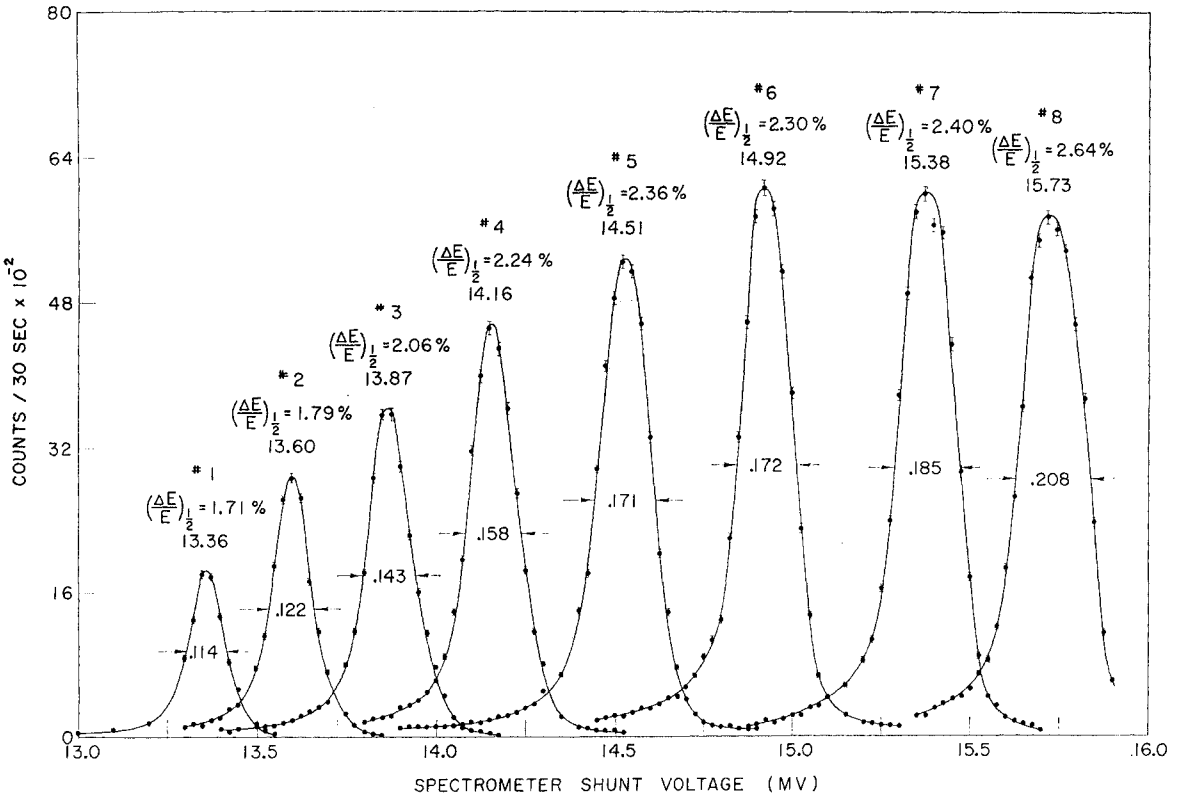

FIG. 1. Cm^{244} 5.81-MeV α-particle momentum spectra.

[21] K. L. Brown, Rev. Sci. Instr. **27**, 959 (1956).
[22] W. C. Barber and V. J. Vanhuyse, Nuclear Phys. **16**, 381 (1960).
[23] G. W. Tautfest and H. R. Fechter, Rev. Sci. Instr. **26**, 229 (1955).
[24] Pilot Chemicals Incorporated, 36 Pleasant Street, Watertown, Massachusetts.
[25] I. A. D. Lewis and F. H. Wells, *Millimicrosecond Pulse Techniques* (McGraw-Hill Book Company, Inc., New York, 1955), Chap 7, p. 232.

background from fast (n,p) events occurring in the scintillators.

The initial electron energy was calibrated both by (γ,n) threshold measurements[22] and by measurements of the energy of elastically scattered electrons with the proton spectrometer. The latter method assumes that the magnetic field configurations for the detection of 40-Mev electrons are the same as those for the detection of 5.81-MeV α particles and differ only in magnitude. The threshold and elastic scattering methods of determining E_0 agreed within 2%.

The method of spectrometer energy calibration with the use of the Cm^{244} 5.81-MeV α-particle source has been described previously.[22] The momentum spectra of the Cm^{244} α particles used for the energy calibration are shown in Fig. 1. The values of $\Delta E/E(=2\Delta p/p)$ are the full width values at half-height.

In order to monitor the performance of the secondary-emission beam-current monitor and the stability and reliability of the counting equipment, signal runs were intersticed with 0.003-in. Al target runs. These Al runs checked the integrated stability of the above components to within the 1.7% counting statistics of a standard Al run. No deviations of SEM performance were measured during these runs nor in the absolute SEM calibration measurements (within 0.3%) using a Faraday cup made 71 days apart. Deviations of 7.5% in the Al yield were observed after angular distribution measurements were made (see Results and Discussion section) and subsequent data (O-energy spectrum below 9.2 MeV) were corrected for this deviation. The absolute SEM response as a function of electron energy is shown in Fig. 2.

The quantity $(\Delta E/E)\Delta\Omega C$, needed for absolute cross-section derivations,[22] where C is the number of electrons-per-unit monitor response, was obtained from the photodisintegration of D by assuming Whetstone and Halpern's[26] cross sections and angular distributions and from the directly measured quantities $\Delta E/E$, $\Delta\Omega$, and C. The spectrometer solid angle $\Delta\Omega$ was measured experimentally and the spectrometer energy acceptance $\Delta E/E$ was calculated from energy calibration formulas and the known spatial separation and width of the scintillators. The measured solid angle $\Delta\Omega$ subtended by

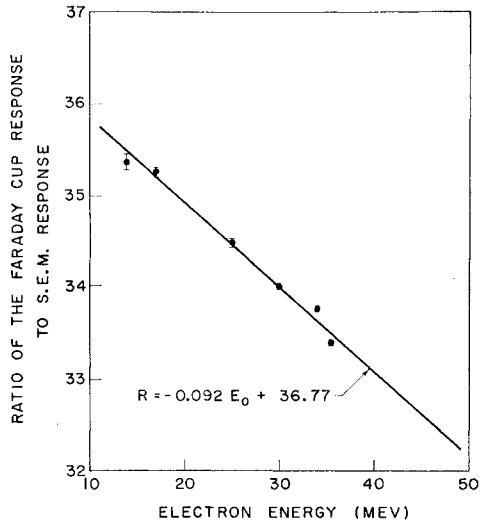

FIG. 2. S.E.M. response as a function of electron energy.

each counter and $\Delta E/E$ for each counter, along with the relative counter efficiencies $(\Delta E/E)\Delta\Omega$ obtained directly and from thick Al-target data, are shown in Table I. The $D(\gamma,p)$ value of $(\Delta E/E)\Delta\Omega C$ was 10% higher than the synthesized value. The value obtained from direct measurements (4×10^9 sr-electrons-per-unit monitor response) was used in our cross-section determinations.

A description of the targets is given in Table II. The gas-target cells used in the Ar, B, O, and Ne experiments were cylinders, 1.875 in. in diam by 2.0 in. in height, with 0.00025-in. 301 stainless-steel walls, gold-silver soldered to thicker stainless-steel ends which contained inlet and outlet ports. Two of these cells, one containing the signal gas and the other H_2 for background measurements and both inflated to approximately equal pressures to ensure nearly identical shapes, were mounted on the spectrometer vertical-transport mechanism, with the cylinder axis contiguous with the scattering-chamber axis and perpendicular to the electron-beam direction. Alternation of the roles of the target and background chambers confirmed the similarity of the two chambers, and, hence, the validity

TABLE I. Solid angle and $\Delta E_p/E_p$ determinations.

Counter	$\Delta E_p/E_p$ (%)	$\Delta\Omega\times10^3$ with Pb baffle	$(\Delta E_p/E_p)\Delta\Omega$ $\times10^5$	$(\Delta E_p/E_p)\Delta\Omega$ $\times10^3$ Norm. to No. 7	$(\Delta E_p/E_p)\Delta\Omega$ $\times10^3$ From Al data	$\Delta\Omega$ ratio with and without Pb baffle	Unbaffled $\Delta\Omega\times10^{-2}$
2	1.23	8.1	10.0	0.59	0.45	0.80±0.06	1.01±0.06
3	1.34	8.5	11.4	0.67	0.57	0.78±0.05	1.09±0.06
4	1.50	8.7	13.1	0.77	0.74	0.75±0.05	1.16±0.06
5	1.74	8.7	15.1	0.90	0.90	0.80±0.04	1.09±0.05
6	1.94	8.7	16.9	1.00	1.00	0.71±0.04	1.22±0.06
7	1.89	9.5	17.9	1.06	1.06	0.83±0.04	1.16±0.05
Mean values	···	8.7±0.4	···	···	···	0.78±0.04	1.11±0.08

[26] A. Whetstone and J. Halpern, Phys. Rev. **109**, 2072 (1958).

TABLE II. Description of targets.

Element	Target	Isotopic composition (%)	Supplier and purity (%)	Actual target thickness (mg/cm²)	Average absolute pressure (lb/in.²)	Target thickness at NTP (mg/cm²)
O	O_2	(99.8) O^{16}	Linde Co.[a] MSC grade (99.99)	6.29	27.8	3.66
F	CF_2	(100) F^{19}	··· (100)	2.55	···	···
Ne	Ne	(90.9) Ne^{20} (0.3) Ne^{21} (8.8) Ne^{22}	Linde Co. MSC grade (99.99)	3.66	25.2	2.31
Ar	Ar	(99.6) Ar^{40}	Linde Co. com'l grade (99.99)	4.79, 6.34	16.8, 22.7	4.56
B	B_2H_6	(18.7) B^{10} (81.3) B^{11}	Bios Labs[b] (unspecified)	···	27.2	···
C	CH	(98.9) C^{12} (1.1) C^{13}	A. D. Mackay[c] (100)	3.54	···	···
Al	Al	(100) Al^{27}	Com'l Al foil	20.6	···	···

[a] Linde Company, Division of Union Carbide Corporation, 22 Battery Street, San Francisco, California.
[b] Bios Laboratories, Incorporated, 17 West 60th Street, New York, New York.
[c] A. D. Mackay, Incorporated, 198 Broadway, New York, New York.

of the background subtraction method, to within 2%. The wall thickness of the chambers was determined indirectly by measuring the energy loss of the Cm^{244} α particles in the chamber walls. At spectrometer angles smaller than approximately 45° or larger than approximately 135° the spectrometer could "see" the portions of the target walls that were struck by the beam. The hydrogen-filled target served to evaluate this background. In order to restrict the region "seen" by the spectrometer, a lead baffle with an opening 0.880 in. wide by 1.975 in. high was placed in the spectrometer entrance port 8.95 in. from the scattering-chamber center. The spectrometer solid angle with the baffle in place was about 20% less than with no baffle, but the great reduction in background (a factor of 5 in some cases) afforded by the baffle made its use desirable. The effective gas-target length was measured for a spectrometer angle of 76° by means of the α-particle source. The source was masked to a 0.06-in. vertical slit, and the counting rate was measured as a function of the displacement along the beam direction of the source from the scattering-chamber center. The resulting "profile" was approximately trapezoidal. The length of a rectangle of the same area and height as the measured trapezoid was 1.01 ± 0.03 in. The effective target thickness at other angles is discussed in Sec. III B.

In most experiments counts were recorded simultaneously in the eight different momentum channels sampled by the eight counters. In taking proton-energy distribution, we varied the spectrometer magnetic field in small steps so that the same proton energy was eventually measured by a number of detectors. The proton energies as determined by the detector position and the spectrometer field setting were corrected for proton-energy losses in the target,[27] and then the results from the different counters were combined into energy bins of less than 1% width. The required relative efficiency $(\Delta E/E)\Delta\Omega$ of each counter was determined from the data taken with the thick aluminum target where the statistical errors were small and the proton-energy spectrum was smooth.

[27] M. Rich and R. Madey, University of California Radiation Laboratory Report-2301, 1954 (unpublished).

III. EXPERIMENTAL RESULTS AND DISCUSSION

A. Excitation and Energy-Distribution Experiments

In most cases we interpreted our (e,pe') excitation-experiment data by assuming that only $E1$ transitions are important in the giant-resonance region. As mentioned previously, the electron virtual-photon spectrum, unlike the real-photon spectrum, depends on the multipole order of the transition induced. Consequently, reaction multipolarities could theoretically be determined by electron-excitation experiments alone and the validity of the assumption of only $E1$ transitions in the giant-resonance region investigated; however, in practice, the electron-excitation method of multipolarity determination is difficult. In particular, electron-induced $E1$ and $M1$ transitions can be separated and identified only if the fractional (γ,p) branching to excited states, and the fractional errors resulting from yield-counting statistics are $\ll 2/[(\omega/\omega'+\omega'/\omega)\lambda-2]$—since the $E1$ and $M1$ virtual-photon spectra are approximately proportional to $(\omega/\omega'+\omega'/\omega)\lambda-2$ and $(\omega/\omega'+\omega'/\omega)\lambda$, respectively, [$\lambda$ is defined in Eq. (4)]—and if higher multipoles do not become important at electron energies high enough to satisfy this criterion.

In addition, $\langle f|\mathbf{J}(\mathbf{k},k_0)|i\rangle$, the matrix element of the current operator between initial nuclear and final nuclear-nucleon states, is evaluated for $|\mathbf{k}|=[p^2+p'^2-2pp'\cos\theta]^{\frac{1}{2}}$ in electron-induced transitions and for $|\mathbf{k}|=\Delta\omega$, the energy transfer, in photon-induced transitions. Deviations of the ratio of the square of $\langle f|\mathbf{J}(\mathbf{k},k_0)|i\rangle$, evaluated for those values of $|\mathbf{k}|$ which are effective in electron-induced transitions, to the square of $\langle f|\mathbf{J}(\mathbf{k},k_0)|i\rangle$, evaluated for the value of $|\mathbf{k}|$ which is effective in photon-induced transitions, from unity must be small for the above considerations to

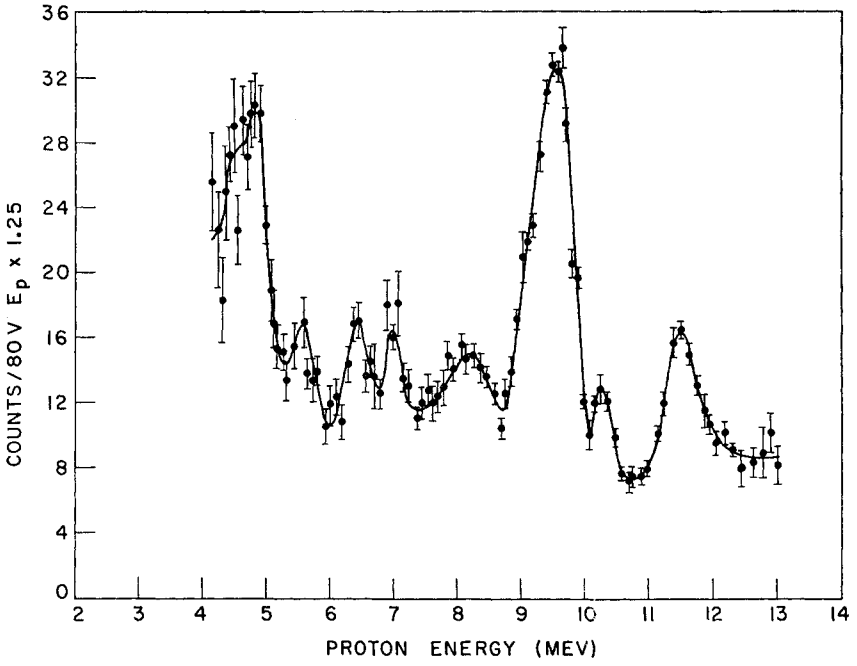

FIG. 3. Oxygen energy spectrum $E_0=30$ MeV, $\theta=76°$.

apply. The stacked-foil experiments of Barber[28] have shown this to be a good approximation for C^{12} for electron energies below ~ 60 MeV.

Experimental instabilities partially nullified the accumulation of enough counting statistics and, in most cases, excited-state branching appeared to be too large to satisfy the above criterion. Therefore, we assumed $E1$ excitation and interpreted deviation of the proton yield from an $E1$ isochromat as attributable to an additional $E1$ transition in which the residual nucleus was left in an excited state. Usually a definite break in the yield curve occurred when deviations were observed, and, since the general $E1$ character of the giant resonance is alleged to be well established, the above assumption is highly plausible. However, our results do not exclude the possibility of other than $E1$ excitation in isolated proton peaks.

3.1 Oxygen

Our experimental results for the O (e,pe') yield (Fig. 3), with an initial electron energy $E=30$ MeV, are in agreement with the gross features of earlier[29] and contemporary[14] (γ,p) work, although our superior resolution and counting statistics enabled us to resolve a small peak at 10.25 MeV on the high-energy side of the large resonance at 9.53 MeV, usually alleged to be the O giant resonance. The energy spectrum at 48° (Fig. 4) confirms the existence of this small peak and extends the spectrum to a proton energy of 14 MeV, showing the smooth yield decrease above the 11.50-MeV peak. Peaks occur at proton energies of 4.85, 5.60, 6.45, 7.00, 8.30, 9.53, 10.25, and 11.50 MeV, corresponding, in the case of ground-state transitions, to photon energies of 17.27, 18.07, 18.99, 19.57, 20.65, 22.30, 23.10, and 24.35 MeV. Geller[30] has applied second-order difference analysis of the bremsstrahlung yields to the $O^{16}(\gamma,n)$ reaction and obtained peaks at 18.11, 18.91, 19.60, 20.70, and 22.4 MeV, the first three consecutive, the last two intersticed between other peaks of unspecified widths. The agreement between peaks in $\sigma(\gamma,p)$ of our experiment and $\sigma(\gamma,n)$ as derived by Geller provides support for charge symmetry of nuclear forces. The $\sigma(\gamma,n)$ of Milone *et al.*[31] at a bremsstrahlung end point energy of 31 MeV is not in agreement with our proton spectra, but because of the statistics of the (γ,n) experiment the difference is probably not significant.

Excitation of the 9.58-MeV O protons (Fig. 5) indicates ground-state transitions up to an excitation energy of 31.8 ± 0.5 MeV, above which approximately 8% of the proton yield leaves the residual nucleus N^{15} with 9.5 ± 0.5 MeV of excitation. Extreme single-particle photonuclear theory[32] requires N^{15} to be left in a state of negative parity and spin $\frac{3}{2}$ or $\frac{1}{2}$. N^{15} levels with unassigned spin and parity exist at 9.16 and 9.81 MeV,[33] and consequently single-particle excitation implies one or both of these levels should be $\frac{1}{2}^-$ or $\frac{3}{2}^-$. Unfortunately the counter system straddled the 10.25-MeV proton peak during excitation experiments; but the straddling counters at 10.00 and 10.55 MeV (Fig. 6) indicated

[28] W. C. Barber, Phys. Rev. **111**, 1642 (1958).
[29] M. Elaine Toms, *Bibliography of Photonuclear Reactions* (Naval Research Laboratory, Washington, D. C., 1958), pp. 31–33.
[30] K. N. Geller, Phys. Rev. **120**, 2147 (1960).
[31] C. Milone and A. Rubbino, Nuovo cimento **13**, 1035 (1959).
[32] W. E. Stephens, A. K. Mann, B. J. Patton, and E. J. Winhold, Phys. Rev. **98**, 839 (1955).
[33] F. Ajzenberg-Selove and T. Lauritsen, Ann. Rev. Nuclear Sci. **10**, 419 (1960).

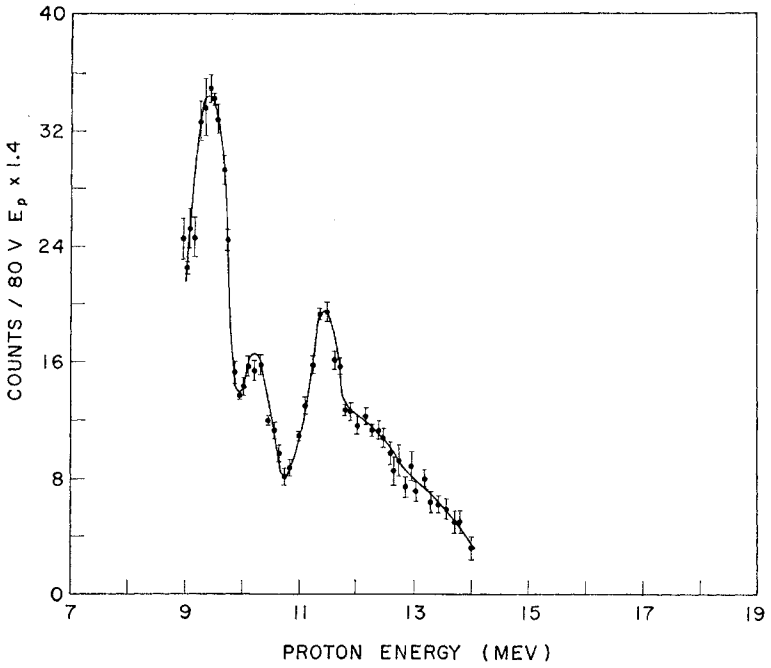

FIG. 4. Oxygen energy spectrum $E_0=30$ MeV, $\theta=48°$.

ground-state transitions for excitation energies up to approximately 33 MeV for the 10.00-MeV protons, and approximately 30±0.5 MeV for the 10.55-MeV group, with about a 25% branching ratio to the 6.33 MeV $\frac{5}{2}^-$ state of N^{15}. However, these counters were on steep portions of the energy distribution and small diurnal spectrometer-field instabilities could have produced large errors in the yield. The 11.50-MeV proton yield (Fig. 5) follows a 24.4-MeV isochromat in the range of excitation energies of this experiment, corresponding to ground-state transitions. The 12.33-MeV protons also leave N^{15} in the ground state (Fig. 7) with slight evidence for excited-state transitions for electron bombarding energies above 34 MeV. Table III summarizes the excitation characteristics of the O protons for E_p greater than 9.53 MeV.

Excitation functions at proton energies lower than 7.5 MeV could have clarified the synthesis of data of other experimental workers by Fuller and Hayward[34] who conjectured that a large fraction of these lower-energy protons were produced by the absorption of photons in the region of 25.2 MeV with the residual nucleus N^{15} left in an excited state. Experimental running-time limitations precluded low-energy proton excitation experiments, but the data synthesized in

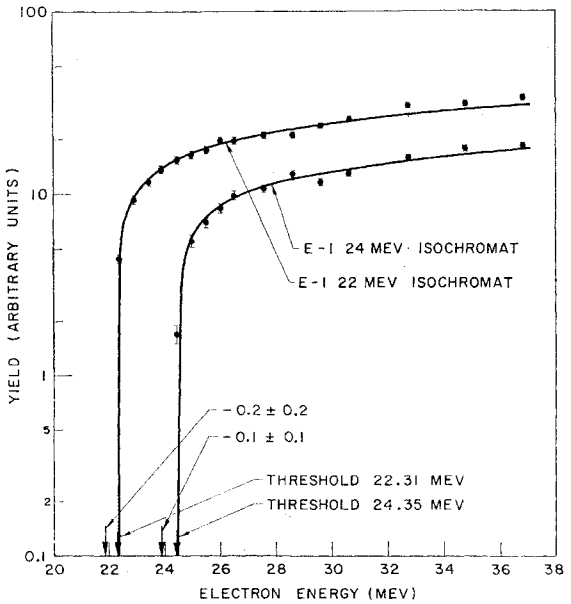

FIG. 5. Excitation functions of 9.6- and 11.5-MeV protons from oxygen.

TABLE III. Summary of the excitation characteristics of the O protons for $E_p>9.53$ MeV.

Proton energy (MeV)	Ground state transition energy (MeV)	Electron energy at which a deviation from an $E1$ isochromat occurs (MeV)	Branching ratio (%)	Energy of excited state (MeV)
9.58	22.31	31.8±0.5	8±8	9.5±0.5
10.55	23.30	30.0±0 5	25±10	6.7±0.5
11.49	24.35	...	...	...
12.33	25.29	34.0	...	...

[34] E. G. Fuller and Evans Hayward, in *Proceedings of the International Conference on Nuclear Structure, Kingston* (University of Toronto Press, Toronto, 1960), pp. 711–712.

reference 39 can be combined with ours to place qualitative limits on the ratio of $(d\sigma/d\Omega)_{76°}$ at photon energies of 22.4 and 25.3 MeV. The unlikely assumption that the entire yield of protons in the 7.3-MeV region is attributable to transitions with the N^{15} left in an excited state leads to an upper limit for the ratio of 1:1. This ratio is insensitive to exactly which excited states are fed because of the relatively flat yield in the region in which the final-state properties of the proton are uncertain. The conclusions above are only valid if none of the protons with $E_p < 5$ MeV are produced by the absorption of 25.2-MeV photons.

The proton radiative capture reaction on N^{15} has been studied by Thomas *et al.*[35] in the photon-energy range of 17.0 to 19.7 MeV, and by Cohen *et al.*[36] for photon energies between 21 and 26 MeV. Discrepancies between the detailed shapes of the experimental (γ,p_0) and (p_0,γ) cross sections do exist, particularly for photon energies in the region of 25 MeV, but elsewhere, except for relative peak size differences, the agreement is fair when the proton energies of the direct reaction are multiplied by the kinematic factor of $[A/(A-1)]^2 = 1.139$ needed for comparison with proton energies of the capture reaction. Detailed balance predicts

$$\left(\frac{d\sigma}{d\Omega}\right)_{\gamma,p_0} = 4M_p c^2 \frac{E_{p_0}}{E_\gamma^2}\left(\frac{d\sigma}{d\Omega}\right)_{p_0,\gamma}, \qquad (5)$$

for O, from which Cohen *et al.* obtained for the 9.53-MeV peak $(d\sigma/d\Omega)_{\gamma,p_0} = 14$ mb/4π sr $= 1.12$ mb/sr at 90°, to be compared with our 1.32 mb/sr.

The integrated cross sections and widths of an approximate resonance curve fit to the data for $22 < E_\gamma < 25$ MeV are given in Table IV. The difficulty in fitting a single resonance curve to the region around 22.3 MeV, and the appearance of a slight inflection on the lower-energy side of this peak suggest unresolved structure. To unfold the contributions of the finite spectrometer resolution and the finite electron-beam width to the intrinsic width of the peaks, we geometrically subtracted twice $\Delta p/p$, which is nonrelativistically $\Delta E/E$, as given by the full width at half-maximum height of the Cm^{244} α-particle momentum spectrum ($\Delta E = 0.024E$ for counter 7; Fig. 1) and algebraically subtracted the proton-energy loss in an electron-beam width of the gas (at experimental temperature and pressure). For the latter correction, we assumed a uniform electron-beam intensity distribution which overestimated the resolution degradation produced by finite

TABLE IV. Parameters of an approximate resonance curve fit to the O cross section for $22 < E_\gamma < 25$ MeV.

Proton energy of peak (MeV)	Photon energy of peak (MeV)	Peak height at 76° (mb/sr)	Photon width at half-height (MeV)	$\int\sigma(\gamma,p)dE_\gamma$ under resonance curve (MeV-mb)	$\%\int_{16.7}^{27}\sigma(\gamma,p)dE_\gamma$
9.53	22.3	1.29	0.70	14.4	26.2
10.25	23.1	0.27	0.32	1.7	3.1
11.50	24.35	0.78	0.87	10.9	19.7
				Total 27.1	49.0

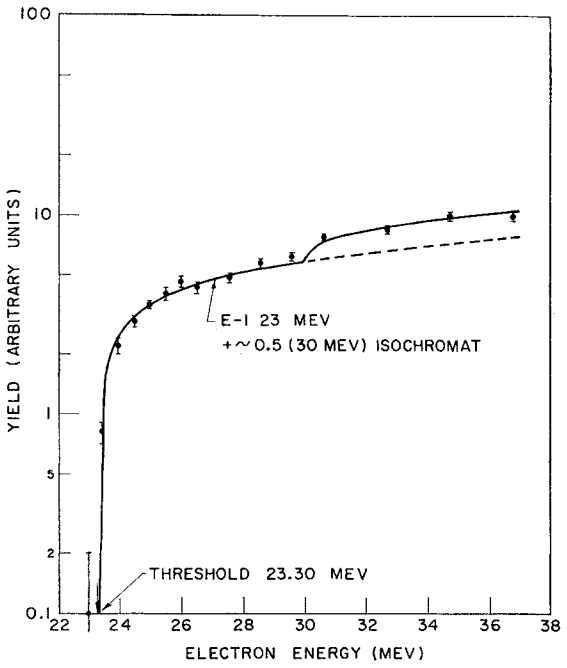

FIG. 6. Average of the excitation functions of 10- and 10.5-MeV protons from oxygen.

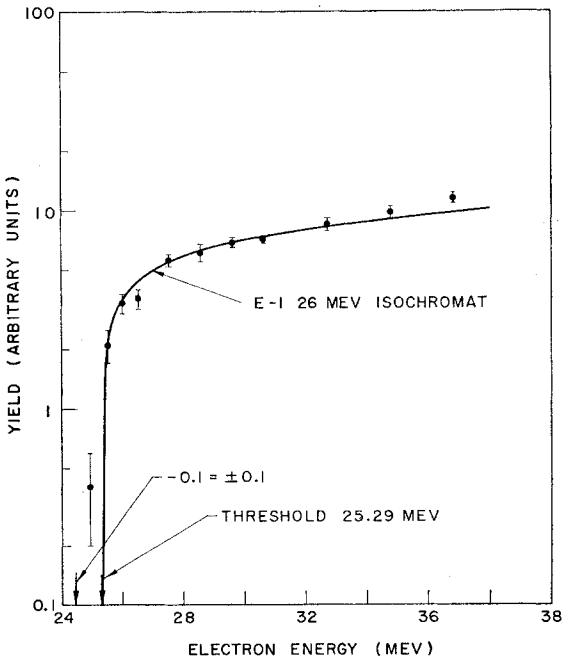

FIG. 7. Excitation function of 12.3-MeV protons from oxygen.

[35] N. W. Tanner, G. C. Thomas, and W. E. Meyerhof, Nuovo cimento 14, 257 (1959).
[36] S. G. Cohen, P. S. Fisher, and E. K. Warburton, Phys. Rev. Letters 3, 433 (1959).

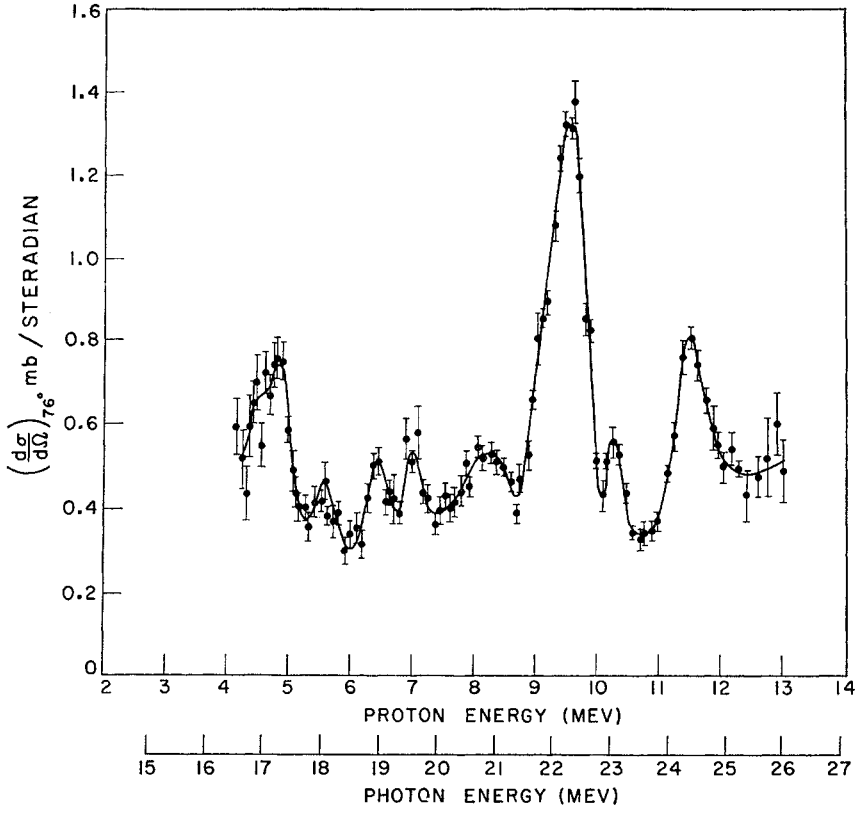

FIG. 8. Oxygen (e,pe') cross section for $E_0=30$ MeV and $\theta=78°$, under the assumption of 100% ground-state transitions.

electron-beam width. With the use of these crude estimates, we find the intrinsic photon widths of the peaks described in Table IV to be 0.62, 0.17, and 0.79 MeV, respectively.

The assumption that only O^{16} (γ,p) transitions occur which leave N^{15} in the ground state for excitation energies up to 30 MeV leads to the differential cross sections at 76 and 48° shown in Figs. 8 and 9. We

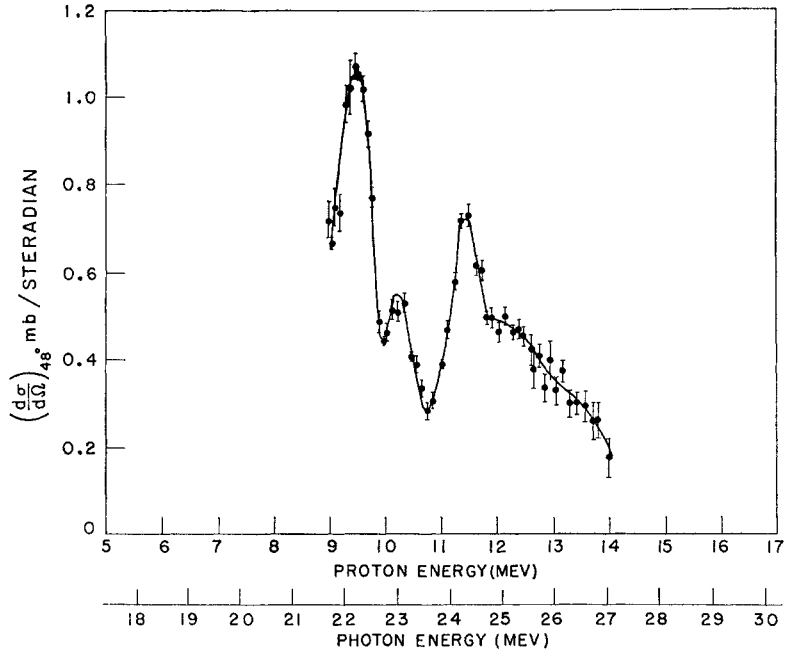

FIG. 9. Oxygen (e,pe') cross section for $E_0=30$ MeV and $\theta=48°$, under the assumption of 100% ground-state transitions.

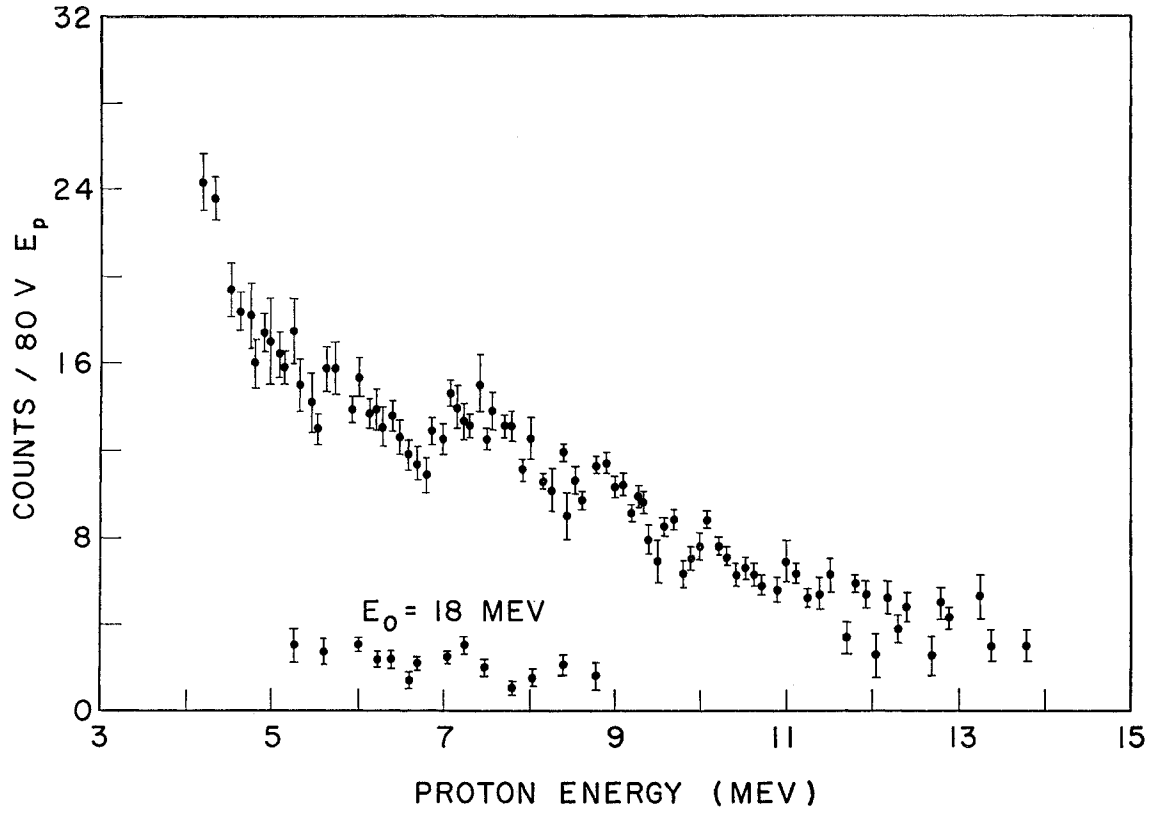

FIG. 10. Fluorine energy spectrum $E_0=30$ MeV $\theta=76°$.

obtained for O^{16}

$$\int_{16.6}^{27}\frac{d\sigma}{d\Omega}(\gamma,p)dE_\gamma=5.4\pm1.1 \text{ MeV-mb/sr at } 76°,$$

or

$$\int_{16.6}^{27}\sigma(\gamma,p)dE_\gamma=56\pm11 \text{ MeV-mb}, \qquad (6)$$

assuming our angular distributions. For O^{16} $\int^{31}\sigma(\gamma,n)dE_\gamma$, Fuchs and Salander[37] obtained 61 ± 7 MeV-mb, while Carver and Lokan[38] obtained 46 ± 7 MeV-mb. These values of $\int\sigma(\gamma,p)dE_\gamma$ and $\int\sigma(\gamma,n)dE_\gamma$ for O are not in serious conflict with the requirements of charge symmetry.

3.2 Fluorine

The F proton energy spectrum was investigated at three initial electron energies, 18, 24.5, and 30 MeV (Figs. 10 and 11). The 24.5-MeV data contain statistically significant peaks at 3.25, 3.7, 4.5, and 7.3 MeV (ground-state-transition photon energies of 11.42, 11.90, 12.74, and 15.70 MeV), while less reliable evidence exists for a considerable amount of fine structure. The 30-MeV spectrum confirms the essential features of the 24.5-MeV spectrum and contains additional structure at higher proton energies, in particular a peak at 10.1 MeV (ground-state-transition energy 18.7 MeV). While the large statistical errors of previous $F(\gamma,p)$ work vitiate a detailed comparison with our results, the agreement in proton energies of the peaks is good. Forkman and Wahlström[39] observed peaks at photon energies of 11.4, 11.9, 12.8, 13.6, 15.4, and 18.1 MeV. The F $\sigma(\gamma,n)$ has not been made with the refined techniques of Geller,[30] but breaks do occur in the $F(\gamma,n)$ activation curves at 11.5, 11.9, 12.2, and 15.3 MeV.[40,41]

No excitation experiments were undertaken *per se*, but the three energy spectra can give semiquantitative final-state information. The yields of the 7.25-MeV F protons at $E_0=18$, 24.5 and 30 MeV are in the proportion of $1/(3.4\pm0.4)/(5.9\pm0.8)$; while $E1$ virtual-photon spectra at these electron energies computed for a momentum transfer corresponding to a transition in which O^{18} is left in the ground state are in the proportion of 1:1.81:3.48. The experimental-yield ratio for

[37] H. Fuchs and C. Salander, in *Contributions to the Karlsruhe Conference, 1960* (Erstes Physikalisches Institut der Universität Heidelberg, Heidelberg, 1961), p. A11.
[38] J. H. Carver and K. H. Lokan, Australian J. Phys. **30**, 312 (1957).
[39] B. Forkman and I. Wahlström, Arkiv Fysik **18**, 339 (1960).
[40] J. G. V. Taylor, L. B. Robinson, and R. N. H. Haslam, Can. J. Phys. **32**, 238 (1954).
[41] J Goldemberg and L. Katz, Phys. Rev. **95**, 471 (1954).

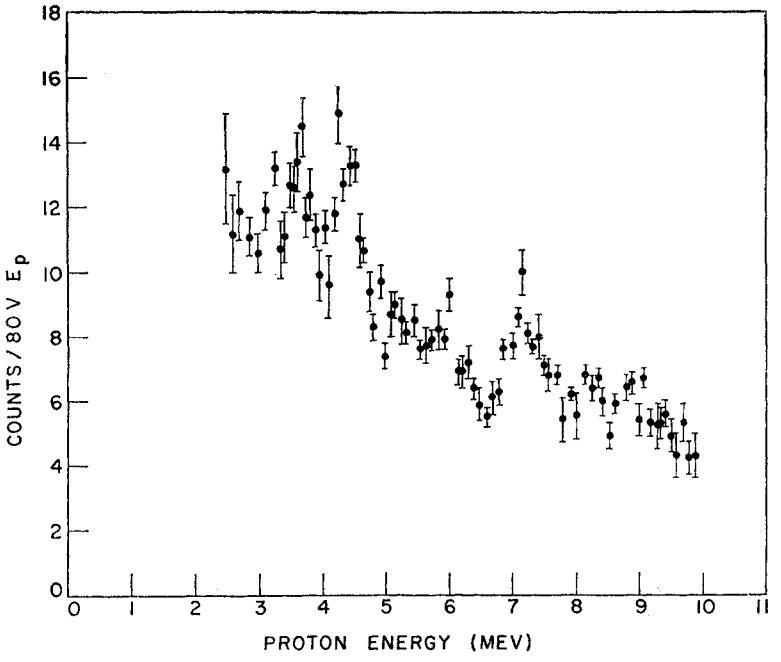

FIG. 11. Fluorine energy spectrum $E_0=24.5$ MeV $\theta=76°$.

electron energies of 30 and 24.5 MeV is 1.7 ± 0.3, while the $E1$ virtual-photon spectra predict a ratio of 1.93. This indicates to first order that the important transitions for 7.25-MeV protons are those in which the residual nucleus O^{18} is left in the ground state or in an excited state with less than 6 MeV of excitation energy. This situation seems to prevail in the energy range where data at the three excitation energies are available. The differential cross section at 76°, derived by making the erroneous assumption of 100% ground-state transitions for illustrative purposes, is given in Fig. 12. The 0^+ ground state, 2^+ 1.98-MeV level, and 4^+ 3.55-MeV level in O^{18} belong to the $d_{\frac{5}{2}}^2$ valence nucleon configuration in the shell-model scheme and thus not expected to be greatly populated by the photonuclear effect, which according to Wilkinson[10] involves predominantly excitation of the closed shell or core nucleons. Several 1^- O^{18} levels below 6 MeV exist which could correspond to hole states of the O^{16} core, but branching ratios to these plausible levels were not

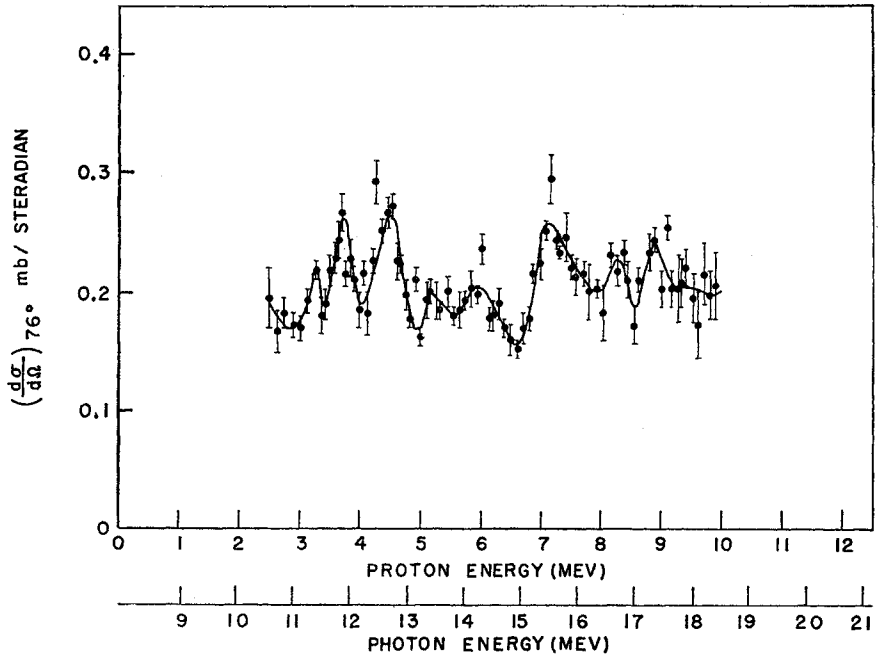

FIG. 12. Fluorine (e,pe') cross section for $E_0=24.5$ MeV and $\theta=76°$, under the assumption of 100% ground-state transitions (known to be erroneous).

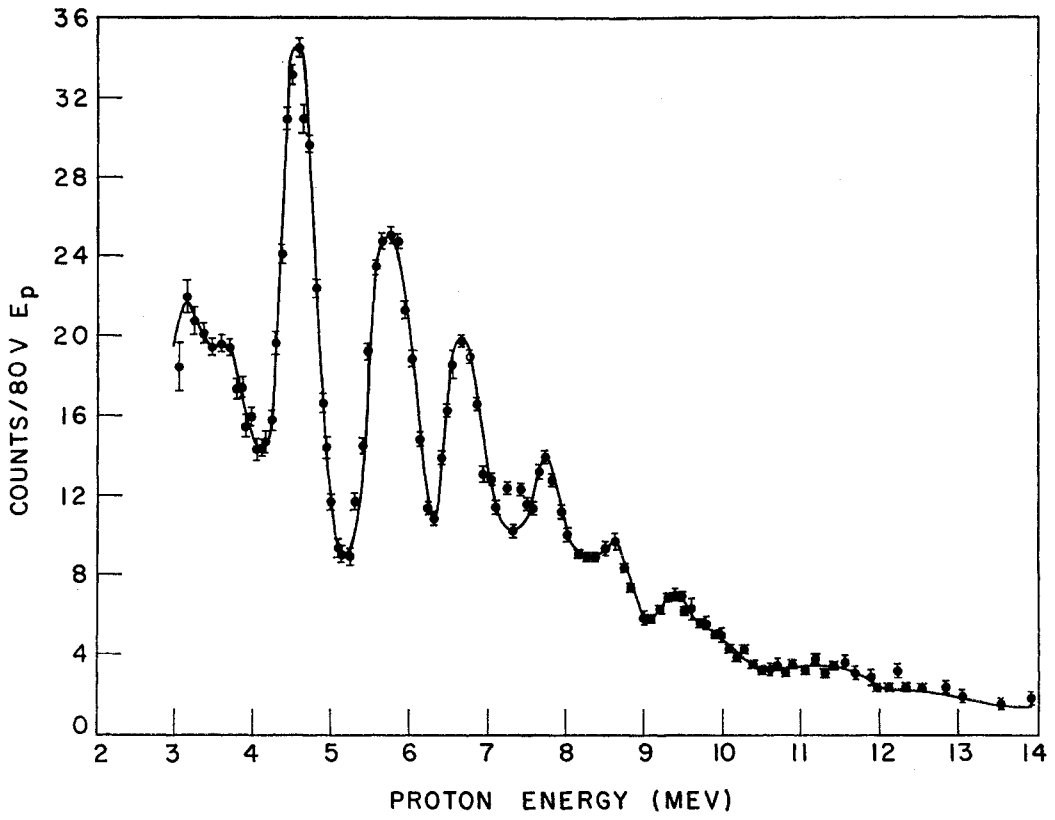

FIG. 13. Neon proton energy spectrum observed with $E_0=30$ MeV and $\theta=76°$.

determined by our experiment. We obtain for F^{19}

$$\int_{10.5}^{23}\sigma(\gamma,p)dE_\gamma=29_{-3}^{+9}\text{ MeV-mb} \tag{7}$$

for the assumption of 100% ground-state transitions, and 37 ± 11 MeV-mb for the assumption that all $F^{19}(\gamma,p)$ transitions leave O^{18} with an excitation energy of 4 MeV. Lasich *et al.*[42] obtained for F^{19}

$$\int_{10}^{16.5}\sigma(\gamma,p)dE_\gamma\approx18\text{ MeV-mb}, \tag{8}$$

which is compatible with our measurements. Ferguson *et al.*[43] obtained for F^{19}

$$\int^{22.2}\sigma(\gamma,n)dE_\gamma=77\text{ MeV-mb}. \tag{9}$$

3.3 Neon

Neon has the most interesting energy spectrum of the elements investigated. The $Ne(\gamma,p)$ reaction was previously investigated with 23-MeV[44] and 80-MeV[45] bremsstrahlung by cloud-chamber measurements of the recoiling F^{19}, but with apparently inconclusive results regarding the shape of the cross section. Warren and Hay,[46] using monochromatic 17.6-MeV photons from the $Li(p,\gamma)$ reaction and a Ne-filled proportional counter, obviously observed the low-energy side of the 4.58-MeV peak but lacked sufficient energy to map the full contour of this peak. Gemmell *et al.*[47] observed the first two peaks in the inverse $F^{19}(p,\gamma_0)Ne^{20}$ reaction, but the peak widths and energies differ from our work which is in excellent agreement with the inverse reaction done at Oxford.[15] We observe narrow, symmetric peaks in the Ne proton-energy spectrum at 76° (Fig. 13) at 3.20, 3.70, 4.58, 5.80, 6.65, 7.75, 8.65, 9.40, and 11.40 MeV, whose envelope has the usual giant-resonance shape with a maximum at 4.58 MeV.

Recent work with nuclear emulsions[48] shows a proton-energy spectrum in excellent agreement with ours.

[42] W. B. Lasich, E. G. Muirhead, and G. G. Shute, Australian J. Phys. **8**, 456 (1955).
[43] G. A. Ferguson, J. Halpern, R. Nathans, and P. F. Yergin, Phys. Rev. **95**, 776 (1954).
[44] J. R. Atkinson, I. Crawford, D. R. O. Morrison, I. Preston, and I. F. Wright, Physica **22**, 1145A (1956).
[45] A. P. Komar and I. P. Iavor, J. Exptl. Theoret. Phys. (U.S.S.R.) **32**, 614L (1957).
[46] J. B. Warren and H. J. Hay, Bull. Am. Phys. Soc. **2**, 178 (1957).
[47] D. S. Gemmell, A. H. Morton, and W. I. B. Smith, Nuclear Phys. **10**, 45 (1959).
[48] K. Shoda (private communication).

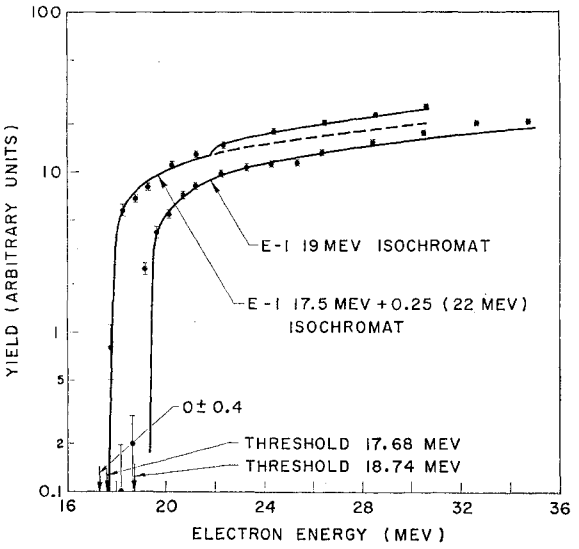

FIG. 14. Excitation functions for the 4.56-MeV and 5.57-MeV protons from Ne.

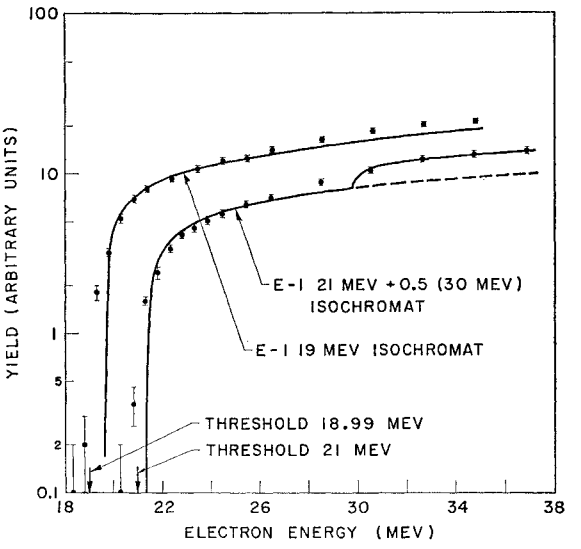

FIG. 16. Excitation functions for the 5.81-MeV and 7.77-MeV protons from Ne.

Attention was focused on the major proton peaks in the Ne-excitation experiments. Unfortunately, even though the experiments were scheduled so that counting statistics for each point on the excitation curve of the major proton peaks were 3% or less, the experimental results cannot be interpreted unambiguously and all the precautions previously cited are especially pertinent to the analysis of the data. In particular, for the reasons explained earlier in this section, the *a priori* assumption of only $E1$ transitions was made, even though there were isolated cases in which the data seemed to be fit somewhat better by $M1$ or $E2$ than by $E1$ virtual-photon isochromats.

Threshold-energy ambiguities arise from three sources: (1) the large primary electron-energy increments of this experiment, (2) the uncertainty in the primary electron-energy calibrations, and (3) the interpretational difficulties that poor threshold statistics and finite electron-energy spread (1.5% full width for all excitation experiments) engender. Because of these difficulties, the important prediction of the independent-particle model that the excited states of the residual nucleus F^{19} predominantly populated by the photo-

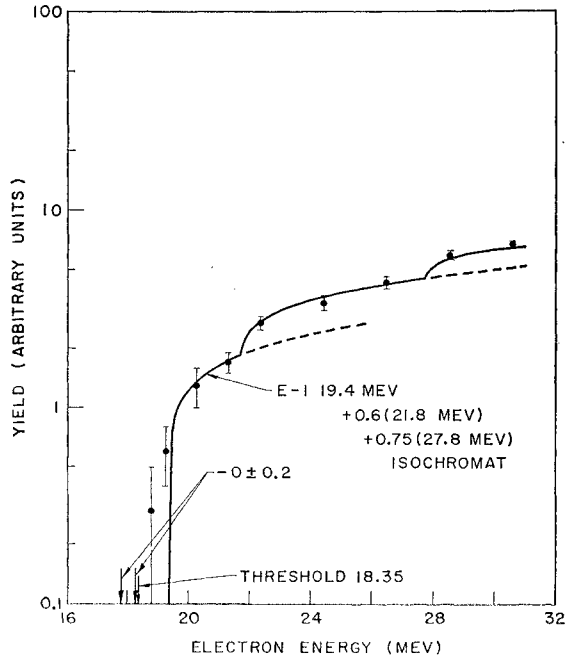

FIG. 15. Excitation function for the 5.20-MeV protons from Ne.

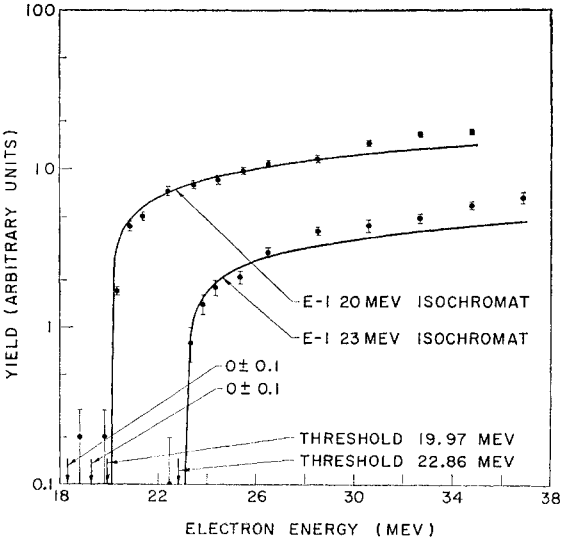

FIG. 17. Excitation functions for the 6.74-MeV and 9.49-MeV protons from Ne.

TABLE V. Summary of the excitation characteristics of the Ne protons.

Proton energy (MeV)	Ground state transition energy (MeV)	Experimental threshold (MeV)	Electron energy at which a deviation from an $E1$ isochromat occurs (MeV)	Branching ratio (%)	Energy of excited state (MeV)
4.56	17.68	17.7±0.3	21.8±0.5	17±8	4.1±0.5
5.20	18.35	19.4±0.6	21.8±0.7; $27.8_{-1}^{+1.3}$	25±5; 39±10	3.5±0.7; $9.5_{-1}^{+1.3}$
5.57	18.74	19.5±0.7	...	...	...
5.81	18 99	19.6±0.6	...	...	...
6.74	19.97	20.0±0.4	...	...	...
7.22	20.47	20.4±0.4	...	...	...
7.77	21.00	21.4±0.5	29.8±1	26±10	8.8±1
8.30	21.61	21.9±0.5	26.0±1	29±10	4.4±1
8.72	22.05	22.3±0.5	26.5±1	29±10	4.5±1
9.20	22.56	23.0±0.6	28.2±1.5	29±10	5.2±1.5
9.49	22.86	23.0±0.5	27.6±1.5[a]	...	4.7±1.5[a]
9.86	23.25	23.6±0.6	...	...	...

[a] Slight evidence.

proton reaction should be $\frac{1}{2}^-$ or $\frac{3}{2}^-$ cannot be ascertained by these excitation experiments alone since the $\frac{1}{2}^+$ ground state and $\frac{1}{2}^-$ first excited state are only 110 keV apart. Presumably, transitions to the other negative-parity states at 1.35 and 1.46 MeV, both with spin $\frac{3}{2}$, could be identified.

The excitation characteristics of the protons from the principal peaks and valleys are displayed in Figs. 14–17, and the salient features, summarized in Table V. The 5.20-MeV protons seem to have a complex parentage with little evidence for ground- or near-ground-state transitions. No excitation experiments were made for the 7.75-MeV peak protons, but since the straddling protons at 7.51 MeV and at 7.94 MeV had experimentally identical yield shapes the results were appropriately combined and presented as the excitation of the 7.77-MeV peak protons. All other excitation curves shown are data from at least two counters lying in a proton-energy interval 1.5% wide, or were data from a single counter.

The differential cross section at 76°, derived with the assumption of 100% ground state transitions, is shown in Fig. 18. We obtained for Ne

$$\int_{16}^{27} \sigma(\gamma,\dot{p})dE_\gamma = 65_{-10}^{+13} \text{ MeV-mb.} \qquad (10)$$

Thomas and Tanner,[15] using detailed balance and normalizing to the work of Farney *et al.*[49] obtained 55

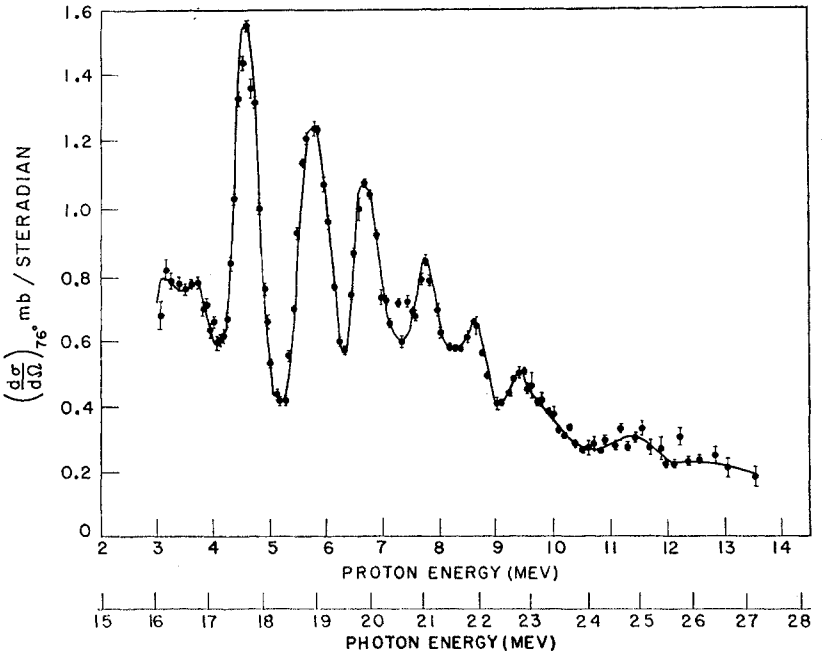

FIG. 18. Neon (e,pe') cross section for $E_0=30$ MeV and $\theta=76°$, under the assumption of 100% ground-state transitions.

[49] G. K. Farney, H. H. Givin, B. D. Kern, and T. M. Hahn, Phys. Rev. 97, 720 (1955).

TABLE VI. Summary of the properties of the major Ne peaks.

Proton energy of peak (MeV)	Photon energy of peak (MeV)	Peak height at 76° (mb/sr)	Photon width at half-height (MeV)	$\int\sigma(\gamma,p)dE_\gamma$ under resonance curve (MeV-mb)	$\%\int_{16}^{27}\sigma(\gamma,p)dE_\gamma$
4.58	17.70	1.45	0.50	11.4	19.0
5.80	18.87	1.11	0.58	11.1	16.7
6.65	19.87	0.90	0.54	7.6	12.7
7.75	21.02	0.77	0.49	6.1	10.5
				Total 36.2	58.9

MeV-mb from the inverse (p,γ) reaction to the ground state of Ne^{20} over essentially the same proton-energy interval. Normalizing to the inverse reaction cross section of Gemmell *et al.*,[47] they obtained 140 MeV-mb. The $\sigma(\gamma,n)$ measurements of Ferguson *et al.*[43] had insufficient resolution to observe structure similar to that occurring in the $\sigma(\gamma,p)$. They obtained, for Ne^{20}, $\int^{21.5}\sigma(\gamma,n)dE_\gamma=52$ MeV-mb. [Because both the ground- and first-excited states of F^{19} have spin $\frac{1}{2}$, and the relative (γ,p) branching ratios to these states are not known, the agreement between the direct and inverse reactions is not necessarily a confirmation of detailed balance; the similarity between the two previous reactions probably stresses the importance of the excitation of discrete levels or very closely spaced groups of levels in Ne^{20} about 1-MeV apart.]

The cross section in the region of the four major peaks can be approximated by a superposition of resonance curves. The width, peak height, area, and integrated cross section of the individual resonance curve belonging to each peak are presented in Table VI. Making the same crude estimates for the contributions of the experimental resolution to the peak width as in the O discussion section results in photon half-widths of 0.46, 0.52, 0.49, and 0.42 MeV, respectively.

3.4 Argon

Our survey study of the $Ar(e,pe')$ energy spectrum at $E_0=30$ Mev, $\theta=76°$ (Fig. 19) exhibits a sharp maximum at a proton energy E_p of 3.6 ± 0.1 Mev, with the yield nearly inversely proportional to E_p from the peak to $E_p=6.8$ Mev, where an inflection occurs in the yield curve. The general features of the energy spectrum are in agreement with the statistically inferior work of Iavor.[50] Since we lack an experimentally determined relationship between photon and proton energy, we can only set limits on the cross section integrated over our proton-energy interval. An isotropic angular distribution is assumed. The assumption of ground-

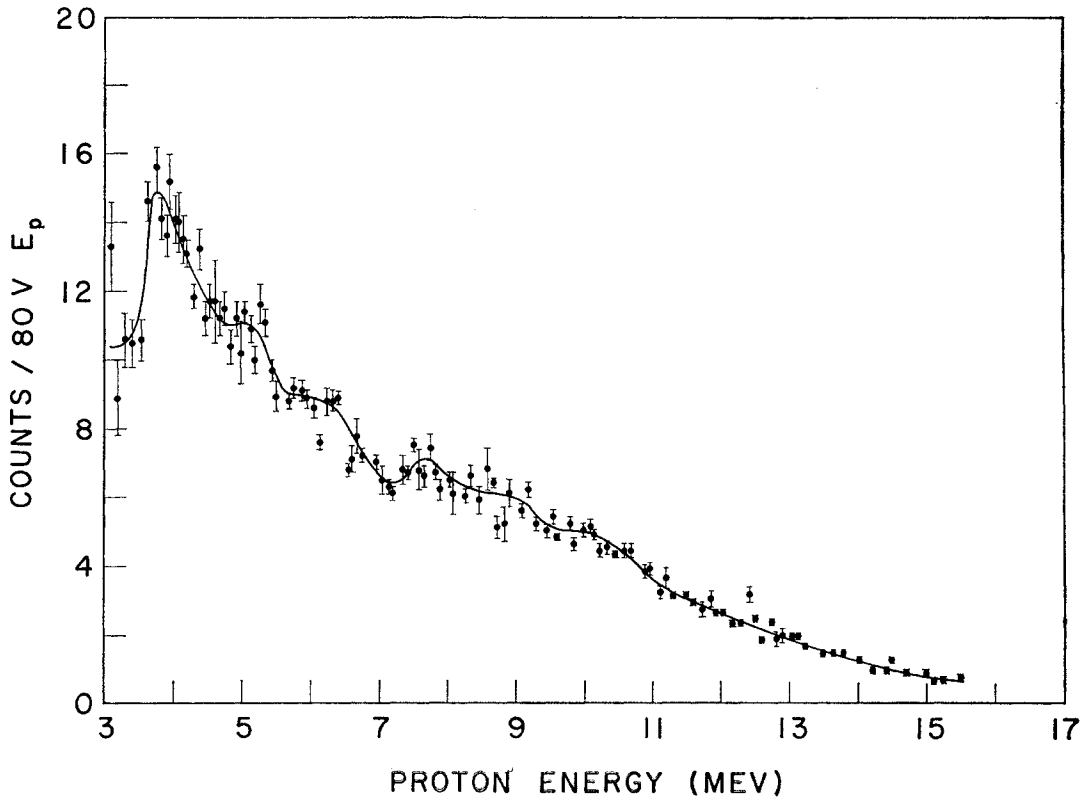

FIG. 19. Argon energy spectrum $E_0=30$ MeV $\theta=76°$.

[50] I. P. Iavor, Soviet Phys.—JETP 7, 983 (1958).

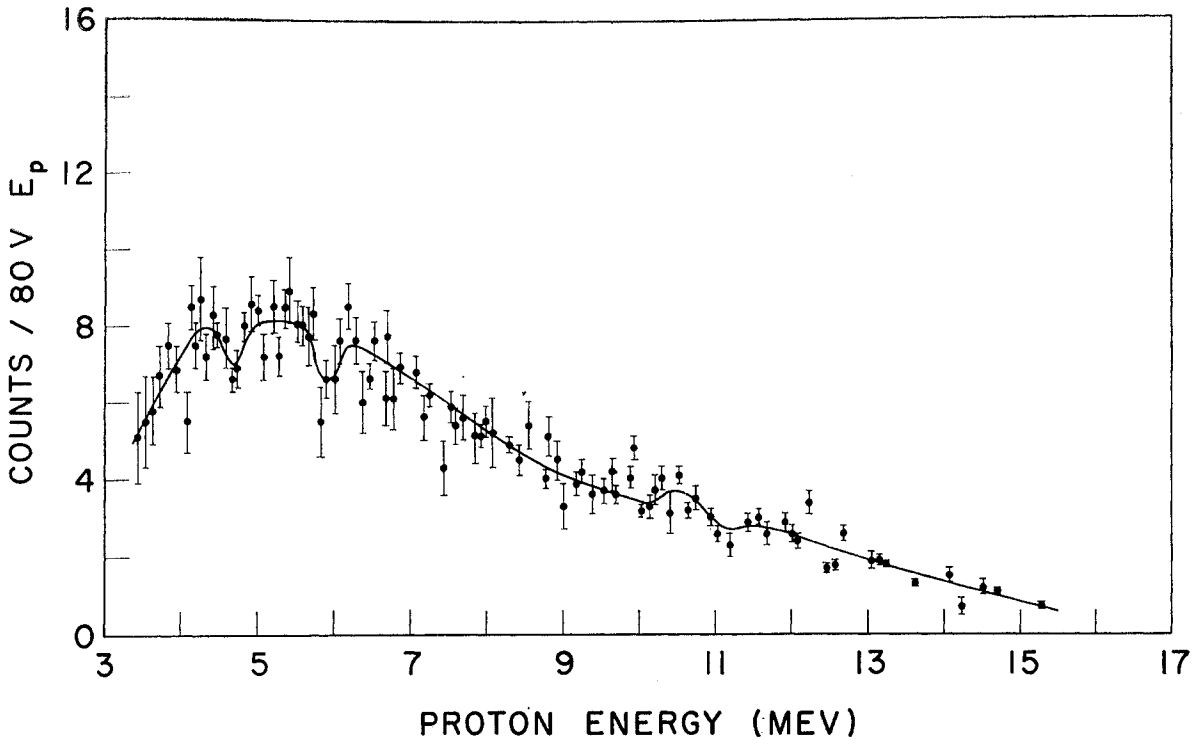

FIG. 20. Boron (e,pe') energy spectrum $E_0=30$ MeV $\theta=76°$.

state transitions, which would make the (γ,p) peak occur at the same photon energy as the (γ,n) peak cross section, leads to 62 MeV-mb; while the assumption that the peak yield arises from the absorption of 24-MeV photons leads to 110 MeV-mb. The latter assumption is supported by the energy spectra of Emma *et al.*[51] taken at bremsstrahlung end point energies of 23, 26, and 30 MeV, and by the shape of $\sigma(\gamma,p)$ measured by Penfold and Garwin.[52] Consequently, we conclude that for Ar^{40}

$$62 \text{ MeV-mb} < \int_{E_p=3.1}^{E_p=15.25} \sigma(\gamma,p)dE_\gamma < 110 \text{ MeV-mb}. \quad (11)$$

Cloud-chamber measurements with $E_{\gamma\max}=15.1$ MeV by Gudden and Eichler,[53] together with estimates of our α-particle counting efficiency, and the continuity of the yields during runs in which the A pressure was changed by a factor of ~ 2 indicate that the large $\sigma(\gamma,\alpha)$ postulated by Emma *et al.* is not observed. If the detected yields had been α particles, the large α-particle energy-loss differences caused by the pressure change would have produced a measurable yield discontinuity.

3.5 Boron

The B energy spectrum at $E_0=30$ MeV (Fig. 20) exhibits a broad maximum centered at 5 MeV with a long high-energy tail. Suggestions of structure appear but statistics do not warrant detailed speculation. Since neither excitation functions nor angular distributions were measured, the B data do not merit extensive discussion. The photoplate work of Erdös *et al.*[54] and estimates of our efficiency for counting deuterons both indicate that most of the yield is protons. In order to provide limits for the B $\int\sigma(\gamma,p)dE_\gamma$, we make a plausible analogy to the F^{19} (γ,p) reaction, assuming that B^{11} and C^{12} (γ,p) reactions are homologous to the F^{19} and Ne^{20} (γ,p) reactions. Using the above analogy, 100% population of the 1^- and 2^- states at 5.96 and 6.26 MeV gives for the B $\int\sigma(\gamma,p)dE_\gamma$ the value 42 MeV-mb. A lower limit is 25 MeV-mb. These estimates are for the proton-energy interval from 3.5 to 15 MeV.

3.6 Carbon

Our C^{12} $\sigma(\gamma,p)$ at $E_0=30$ MeV (Fig. 21) shows the giant resonance peak at $E_p=6.05$ MeV, with slight evidence for structure at 6.7 and 7.2 MeV but with no evidence for splitting of the magnitude observed by Cohen *et al.*[55] The width of the C^{12} (γ,p) giant resonance at half-maximum is approximately 3.1 MeV which is slightly narrower than previously reported.[56] Some

[51] V. Emma, C. Milone, R. Rinzivillo, Nuovo cimento **14**, 62 (1959).
[52] A. S. Penfold and E. L. Garwin, Phys. Rev. **114**, 1139 (1959).
[53] F. Gudden and J. Eichler, Z. Physik **150**, 1139 (1959).
[54] P. Erdös, P. Scherrer, and P. Stoll, Helv. Phys. Acta **26**, 207 (1953).
[55] L. Cohen, A. K. Mann, B. J. Patton, K. Reibel, W. E. Stephens, and E. J. Winhold, Phys. Rev. **104**, 108 (1956).
[56] V. J. Vanhuyse and W. C. Barber, Nuclear Phys. **26**, 233 (1961).

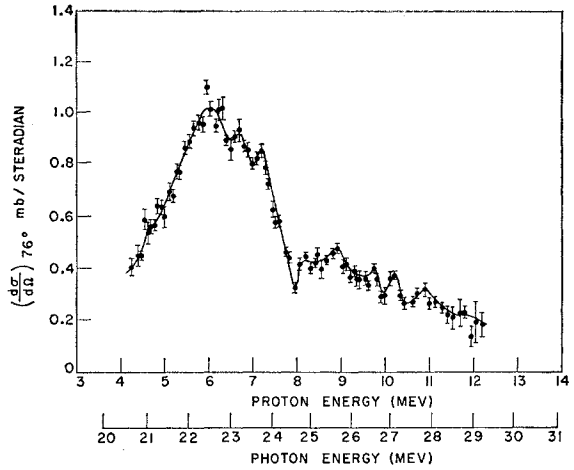

FIG. 21. Carbon (e,pe') cross section for $E_0=30$ MeV and $\theta=76°$, under the assumption of 100% ground-state transitions.

evidence for fine structure exists at proton energies of 8.2, 8.9, 10.2, and 10.9 MeV in the 30-MeV data. The energy spectrum at 24.5 MeV (Fig. 22) again gives us no evidence for splitting; and above proton energies of 8 MeV, where proton emission is energetically impossible, it demonstrates the validity of the background-subtraction method employed. The cross section for $E_0=24.5$ MeV (Fig. 23) is in essential agreement with the 30-MeV cross section, as expected, since the precise work of Penner and Leiss[57] showed an excited-state cross section of $(7\pm16)\%$ of the ground-state cross section for photon energies below 30 MeV. We obtained a differential cross section of 1.03 mb/sr at 76° at $E_p=6.05$ MeV, and

$$\int_{20.3}^{29.3}\sigma(\gamma,p)dE_\gamma=50\pm8 \text{ MeV-mb} \qquad (12)$$

for C^{12}. Using detailed balance, Gemmell *et al.*[58] obtained 24 ± 5 mb for the peak cross section from the inverse $B^{11}(p,\gamma)C^{12}$ reaction. This value becomes 19 ± 4 MeV-mb after converting from the isotropic angular distribution Gemmell *et al.* assumed to a $1+\frac{3}{2}\sin^2\theta$ angular distribution (a factor of $\frac{4}{5}$ for an angular distribution measured at 90°). However, as pointed out in the discussion of the Ne results, the $F^{19}\sigma(p,\gamma_0)Ne^{20}$ of Gemmell *et al.*, obtained with the use of detailed balance, is also about a factor of two larger than our value or the inverse cross section of Thomas *et al.*[15] when the latter used an independent calibration. Gove *et al.*[59]

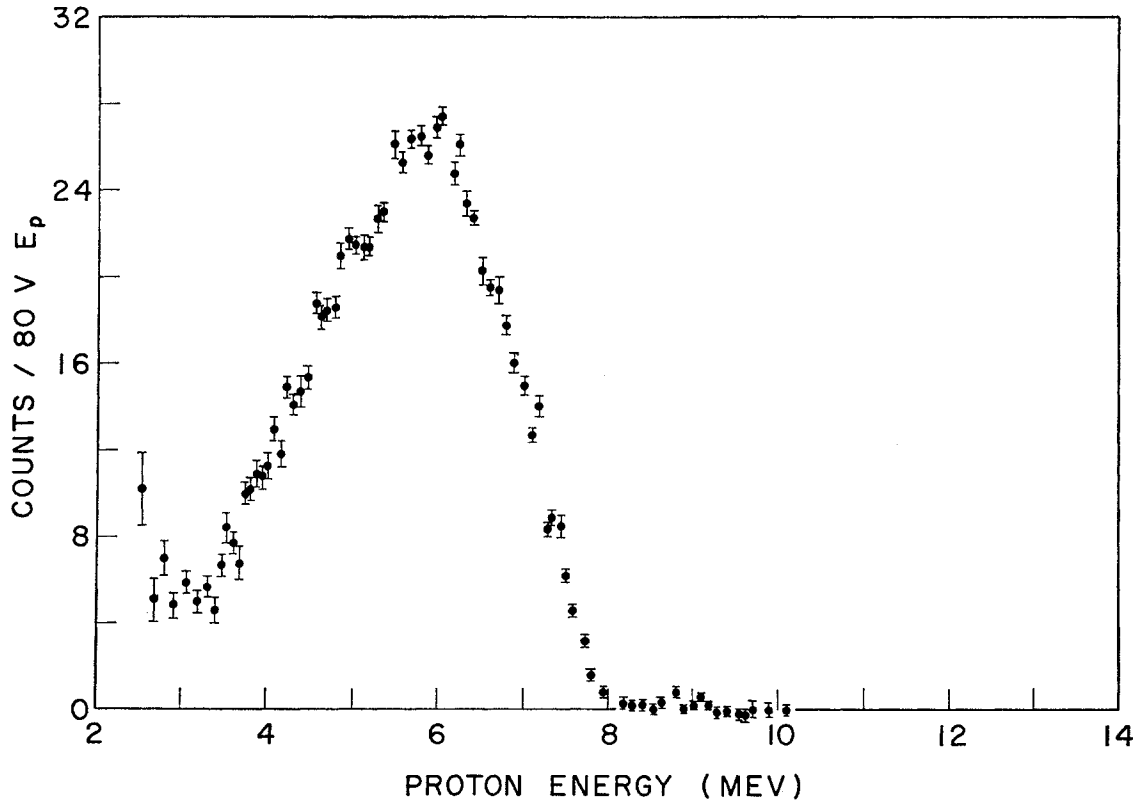

FIG. 22. Carbon energy spectrum $E_0=24.5$ MeV $\theta=76°$.

[57] S. Penner and J. E. Leiss, Phys. Rev. **114**, 1101 (1959).
[58] D. S. Gemmell (private communication).
[59] H. E. Gove, A. E. Litherland, and R. Batchelor (to be published).

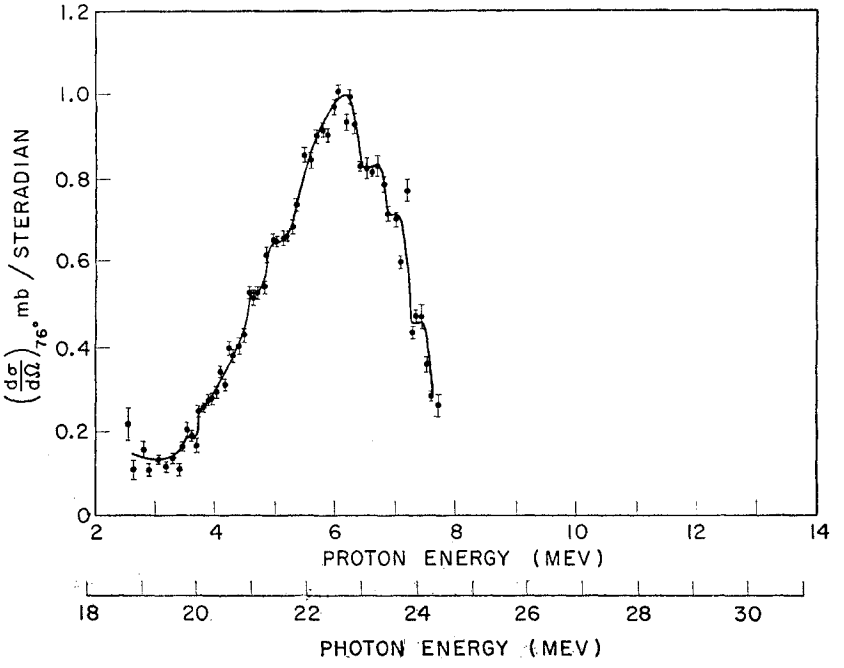

FIG. 23. Carbon (e,pe') cross section for $E_0=24.5$ MeV and $\theta=76°$, under the assumption of 100% ground-state transitions.

have obtained 12 mb for the peak cross section at $E_p=6.05$ MeV from the inverse reaction, while our value is $11.0\pm15\%$ mb for a $1+\frac{3}{2}\sin^2\theta$ angular distribution, or 9.6 mb using the least-squares fit coefficients to our 5.90-MeV C^{12} angular distribution, properly normalized to the peak $d\sigma/d\Omega$.

3.7 Aluminum

The Al proton energy spectra from a 20.6-mg/cm² foil of commercial purity (99% Al) used to monitor the stability and reliability of the experimental apparatus as previously explained are shown in Figs. 24 and 25 for $E_0=18$, 24.5, and 30 MeV. As in the case of F, comparison of the yield ratios at the three primary electron energies with the ratios of $E1$ virtual-photon isochromats enabled us to establish a semi-quantitive relationship between k and E_p (see Table VII). The relationship $k=(27/26)E_p+16$ seems appropriate in the proton-energy interval of 3.4 to 6–7 MeV. Beyond proton energies of 7 MeV, $k=(27/26)E_p+14$ seems

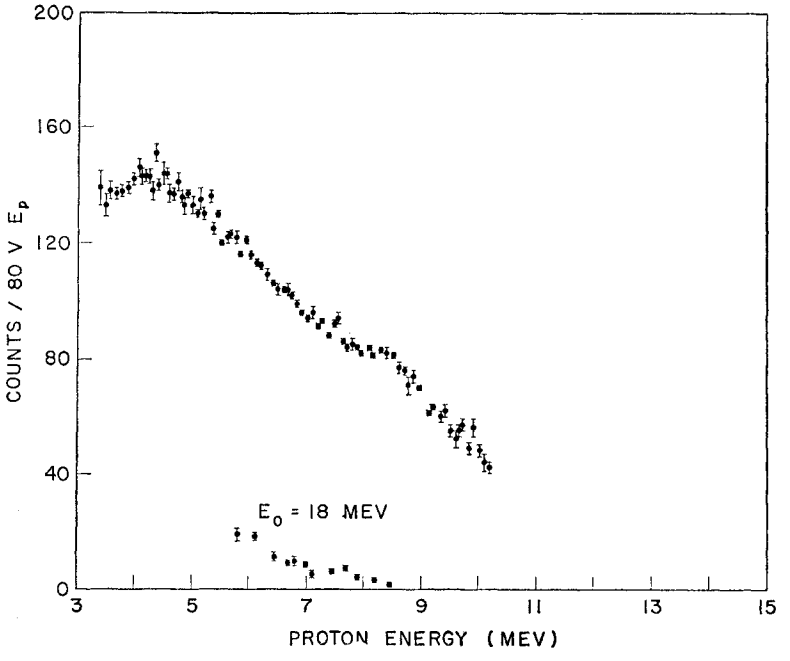

FIG. 24. Aluminum energy spectrum $E_0=24.5$ MeV $\theta=76°$, target thickness 20.6 mg/cm².

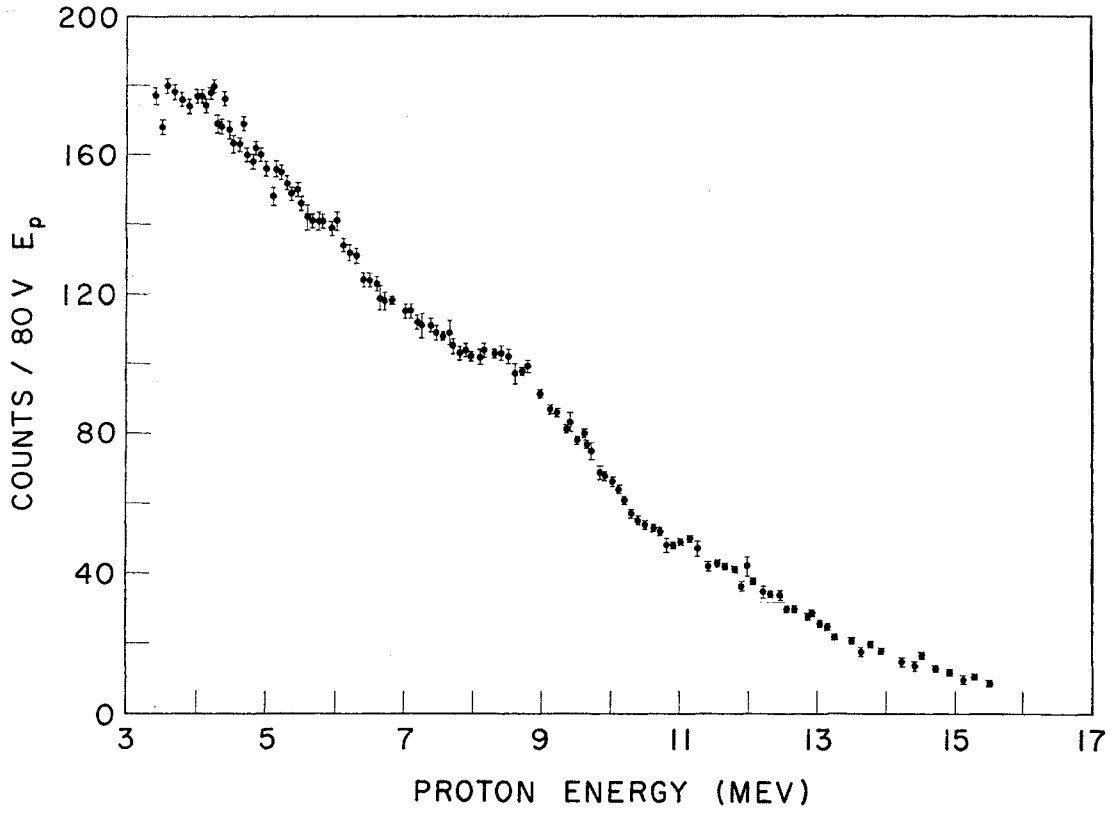

FIG. 25. Aluminum energy spectrum $E_0=30$ MeV $\theta=76°$, target thickness 20.6 mg/cm².

indicated. For simplicity, the assumption that $k=(27/26)E_p+14$ over the entire range of proton energies was made to compute the cross section shown in Fig. 26; the errors are derived from counting statistics only and do not include the uncertainty in the relationship between k and E_p. In any event, the available information does not justify a more sophisticated analysis. The previous experiments of Diven and Almy[60] and those of Dawson[61] had neither the resolution nor the statistics to detect the hump we observed in the region of 8 MeV. However, our work is in agreement with the gross features of their results. We obtained for Al^{27}

$$\int_{18.5}^{29}\sigma(\gamma,p)dE_\gamma=94\pm19\%\ \text{MeV-mb}, \qquad (13)$$

with the use of our angular distribution data. Dawson, using Halpern and Mann's[62] data for calibration, ob-

TABLE VII. Comparison of Al yield at primary electron energies of 18, 24.5, and 30 MeV.

Proton energy (MeV)	Yield $E_0=18$ (MeV)	Yield $E_0=24.5$ (MeV)	Yield $E_0=30$ (MeV)	Yield (24.5) / Yield (18)	Yield (30) / Yield (24.5)	$\frac{N_{E-1}(30,k)}{N_{E-1}(24,k)}$ $[k=(27/26)E_p+16]$	$\frac{N_{E-1}(30,k)}{N_{E-1}(24,k)}$ $[k=(27/26)E_p+14]$
5.19	···	130±2	205±2	···	1.58±0.06	1.52	···
5.60	···	122±2	193±2	···	1.59±0.06	1.54	···
6.02	18.0±1.5	115±2	180±2	6.5± 0.6	1.56±0.06	1.58	···
6.53	11.0±1.5	104±2	170±2	9.5± 1.0	1.64±0.06	1.73	···
7.01	8.5±1.0	94±2	155±2	11.0± 2.0	1.65±0.06	···	1.52
7.47	6.3±0.8	88±2	149±2	14.0± 2.0	1.69±0.06	···	1.54
7.94	4.4±0.8	82±2	140±2	19.0± 3.0	1.71±0.06	···	1.58
8.45	1.2±1.0	82±2	142±2	68.0±57.0	1.73±0.06	···	1.73
8.91	···	72±2	130±2	···	1.81±0.07	···	1.91
9.39	···	62±2	110±2	···	1.78±0.07	···	2.11

[60] B. C. Diven and G. M. Almy, Phys. Rev. **80**, 407 (1950).
[61] W. K. Dawson, Can. J. Phys. **34**, 1480 (1956).
[62] J. Halpern and A. K. Mann, Phys. Rev. **83**, 370 (1951).

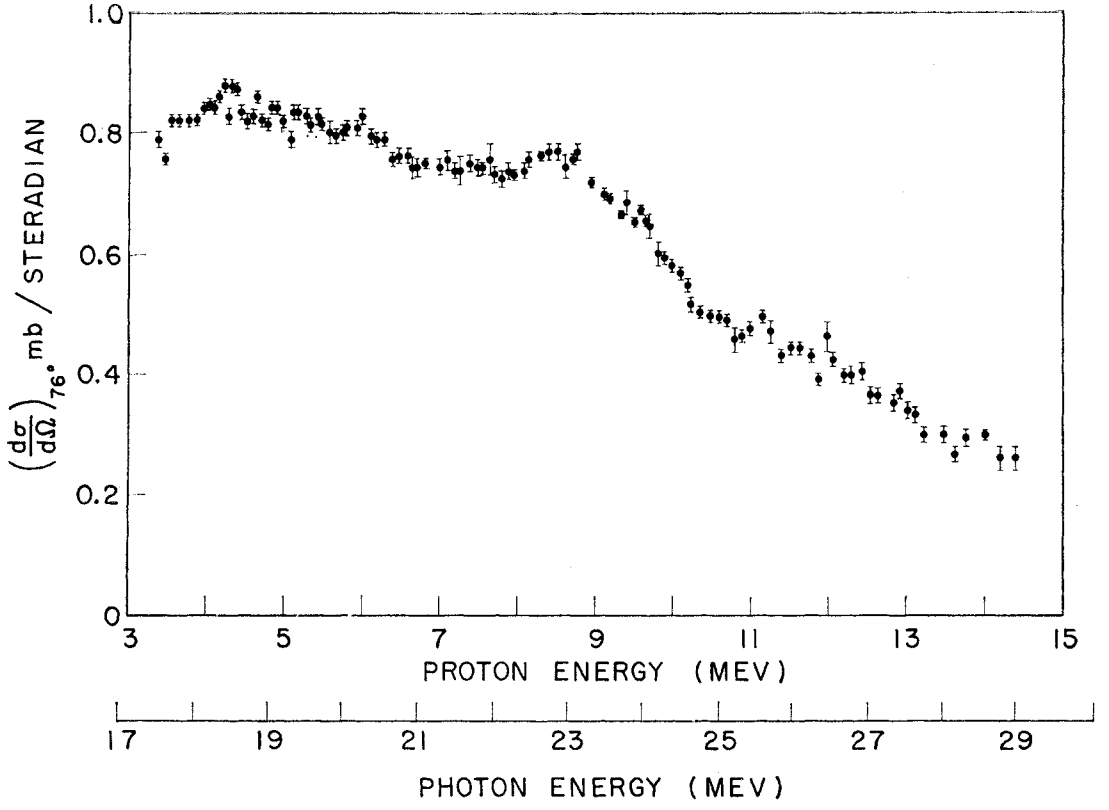

FIG. 26. Aluminum (e,pe') cross section for $E_0=30$ MeV and $\theta=76°$, assuming $k=(27/26)E_p+14$ MeV.

tained $\int\sigma(\gamma,p)dE_\gamma=120\pm30$ MeV-mb, with unspecified photon limits but presumably over the entire range of sensibly nonzero cross section. For Al $\int_{13}^{18.5}\sigma(\gamma,n)\times dE_\gamma$, Baglin *et al.*[63] measured 28 MeV-mb. Since the proton thickness of our Al target was great enough to partially obscure any interesting fine structure, the energy spectrum will not be discussed further; however, the suggestion of unresolved structure, especially at 8 MeV, together with the alleged structure in the total photon absorption curve and the calculations of Baglin *et al.* are intriguing; and perhaps future Al(γ,p) experiments with thinner targets are advisable. On the other hand, our isotropic angular distributions suggest a statistical emission process and smooth absorption cross section.

B. Angular-Distribution Measurements

3.8 The Effective Gas-Target Thickness as a Function of Spectrometer Angle

In order to interpret the angular-distribution data, the effective gas-target thickness as a function of spectrometer angle had to be known. This function was calculated from the geometry of the target diameter and the "profile" of the spectrometer as measured with the α source at the one angle of 76°. The function also depends slightly on the width of the primary electron beam. Details of the calculation are given by Dodge.[64] These calculated relative-target thicknesses have an accuracy compatible with the errors from counting statistics; but for a more precise determination of the former quantities, a comparison of the angular distribution of carbon photoprotons from a CH (polystyrene) foil and methane (CH_4) in the gas chamber would be preferred. This measurement would correspond to the comparison of the angular distributions from a point and an extended source and would eliminate uncertainties caused by a possible $\Delta p/p$ dependence of $\Delta\Omega$ for source positions perpendicular to the magnet symmetry plane.

The electron beam was carefully centered on the gas target at each angle to avoid geometric uncertainties. This slight repositioning of the beam direction at each angle unfortunately *could* have been the cause of an even larger error than was avoided, since the SEM efficiency, after angular distributions were measured, apparently had increased by 7.5%. However, since detailed experimental verification of the SEM's malfunction is lacking, no correction was made. The effect of the alleged SEM efficiency change on the O and Ne

[63] J. E. E. Baglin, M. W. Thomas, and B. M. Spicer, Nuclear Phys. 22, 207 (1961).

[64] W. R. Dodge, Stanford University, High-Energy Physics Laboratory Tech. Rept. No. 246, 1961 (unpublished).

$d\sigma/d\Omega$ data would be to decrease the forward and increase the backward asymmetries. The conclusions based on a comparison of the O and Ne $d\sigma/d\Omega$ would not be altered, since the data were taken consecutively at each angle.

Angular distributions of the prominent peaks in Ne and O were made by successively positioning the peaks on the same counter by taking partial energy distributions at each angle to locate the peaks. The spectrometer field values which were used for the gaseous elements' angular distributions gave nearly the same proton energies after conversion from laboratory to center-of-mass energies. The center-of-mass proton kinetic energy T_{p_0} is related to the laboratory kinetic energy T_p by

$$T_{p_0}=\frac{[1+(k/M_A)][T_p+M_p]-P_p k\cos\theta_{\rm lab}}{[1+(2k/M_A)]^{\frac{1}{2}}}-M_p$$
$$\approx T_p-[kM_p/M_A][2T_p/M_p]^{\frac{1}{2}}\cos\theta_{\rm lab}, \quad (14)$$

where M_A is the mass of the target nucleus, k is the energy of the photon inducing the reaction, and natural units are used. The small spread in the calculated center-of-mass energies as a function of angle gives credence to the assumption that most of the detected particles are protons and is a measure of the accuracy of the location of the peaks. (For the 9.53±0.04 MeV peak in O, the center-of-mass energies were 9.51 MeV, 20°; 9.53 MeV, 48°; 9.55 MeV, 76°; 9.61 MeV, 104°; 9.52 MeV, 132°; and 9.47 MeV, 160°. The energies of the largest two neon peaks were similarly determined on the basis of reproducibility to be located at 4.59±0.03 and 5.79±0.02 MeV.) Because the energies of the angular-distribution data points for the solid targets and for the gaseous targets from counters other than the one which followed the peak under observation were a slight function of the spectrometer angle, the data points were corrected to the value of the cross section corresponding to the average center-of-mass kinetic energy $T_{\rm lab}$ by referring to the cross section at 76°. The correction was largest for those elements whose cross section changed rapidly with proton energy and was approximately 10% in the extreme cases at the extreme angles. The uncertainty of this correction was incorporated in the angular-distribution data errors.

The angular distributions' even-parity terms, which are assumed to arise entirely from an $E1$ interaction, have been corrected for the dependence of the $E1$ virtual-photon spectrum on the reaction product angle [Eq. (4)]. Therefore, if the (e,pe') angular distribution has the form

$$A+B\cos\theta+C\sin^2\theta+D\sin^2\theta\cos\theta, \quad (15)$$

the quantities

$$A'=A-\left[C\frac{\omega'}{\omega}\Big/\left(\frac{\omega^2+\omega'^2}{\omega\omega'}\lambda-2-\frac{3}{2}\frac{\omega'}{\omega}\right)\right] \quad (16)$$

and

$$C'=\left[C\left(\frac{\omega^2+\omega'^2}{\omega\omega'}\lambda-2\right)\right]\Big/\left[\frac{\omega^2+\omega'^2}{\omega\omega'}\lambda-2-\frac{3}{2}\frac{\omega'}{\omega}\right] \quad (17)$$

should be the same as the respective even-parity terms of the real-photon-induced angular distribution. The odd-parity terms, attributable to interference between $E1$ and $E2$ transitions, were not corrected for the dependence of the $E2$ virtual-photon spectrum on reaction-product angle.

The angular distributions were not corrected for finite angular resolution of the spectrometer since this correction was very small. It can be shown, that for a spectrometer of finite horizontal acceptance angle 2Δ, the assumed angular distribution [Eq. (15)] is transformed to

$$A+C\sin^2\Delta+(B\cos\Delta+\tfrac{1}{2}D\sin\Delta\sin2\Delta)\cos\theta$$
$$+C(1-\tfrac{4}{3}\sin^2\Delta)\sin^2\theta+D\cos\Delta\cos2\Delta\sin^2\theta\cos\theta. \quad (18)$$

For a magnetic spectrometer,

$$\tan\Delta=W/S_0[1+(1/n)(r_0/S_0)^2]^{\frac{1}{2}}, \quad (19)$$

where W is the accessible horizontal aperture half-width, S_0 is the distance from the source to the spectrometer entrance, n is the usual magnetic field index, and r_0 is the central radius of curvature. For an $n=\frac{1}{2}$ spectrometer,

$$\tan\Delta=(\Delta\Omega/\Lambda)^{\frac{1}{2}}, \quad (20)$$

where Λ is the ratio of the magnet aperture height to width. In the case of this experiment $\tan\Delta=0.03$; so this correction is negligible.

3.9 Discussion of the Angular Distributions

The O, F, Ne, C, and Al angular-distributions data were fitted to a $\cos\theta$ power series of fourth degree by the least-squares method and the results expressed in the form of Eq. (15) and $\sum_{l=0}^{3}C_lP_l(\cos\theta)$. The even-parity terms of Eq. (15), A and C, were then corrected to photoproduction [Eqs. (19) and (20)]. In our experi-

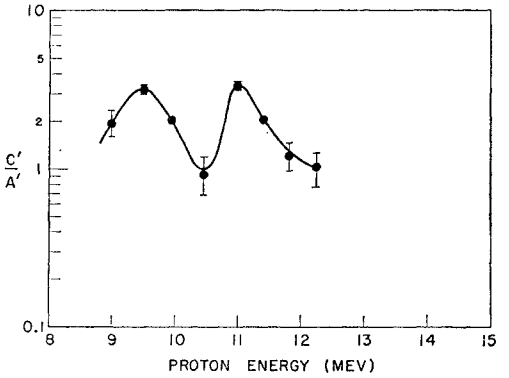

FIG. 27. Ratio of the even-parity terms in the angular distributions of protons from oxygen.

ment there are few examples in which the conversion to photoproduction or the difference between the center-of-mass and the laboratory systems is statistically discernible.

(*a*) *Oxygen.* The O $d\sigma(\gamma,p)/d\Omega$ has been studied in this energy range by Johannson *et al.*,[12] Milone *et al.*,[65] and Brix and Mashke[66]; but the accuracy of previous experiments has been limited by experimental[66] or statistical uncertainties.[12,65] Ratios of C'/A' range from 1.1 obtained by Johannson *et al.* to 6.7 obtained by Brix and Mashke for $E_p>10$ MeV. Our values of C'/A' are shown in Fig. 27. The $d\sigma/d\Omega$ of O protons from the 9.53 and 11.50-MeV peaks and the valley in between are displayed in Fig. 28. Wilkinson's resonance direct mechanism predicts $C'/A'=\frac{3}{2}$ for both the $lp_{\frac{3}{2}}$ to $ld_{\frac{5}{2}}$ transitions and the $lp_{\frac{3}{2}}$ to $ld_{\frac{3}{2}}$ transitions which are expected to be responsible for the 9.53- and 11.50-MeV peaks, respectively. Admixtures of transitions where the relative angular momentum of the proton l changes to $l-1$ with the transitions where l changes to $l+1$, which contribute most of the dipole strength can modify the simple estimates for C/A of Courant[67] and Wilkinson,[6] since the radial matrix elements cannot be factored out of the angular expressions in these cases.[68] Calculations of the expected modification of C'/A' have not been made for oxygen. Figure 29 shows that the asymmetry in O $d(e,pe')/d\Omega$ shifts from the backward to the forward hemisphere, respectively, for protons from the low- and high-energy sides of the 9.53-MeV peak. As Gove[69] has pointed out, this behavior is expected if the asymmetry term arises from interference of two proper Breit-Wigner resonances, one with $J\pi=1^-$ and the other with $J\pi=2^+$, and whose spacing is greater than their widths to ensure the physical reasonableness of the single-level Breit-Wigner approximation. The inelastic electron-scattering experiments of Bishop and Isabelle[70] indicate the presence of an $E2$ level in this vicinity of the photon-absorption cross section. Brown and Levinger[71] have placed an upper limit on σ_{E2}/σ_{E1} of $p^2/20$, where $p=C/D$. For O this formula predicts $\sigma_{E2}/\sigma_{E1}<1.8\%$ for the proton energy interval investigated.

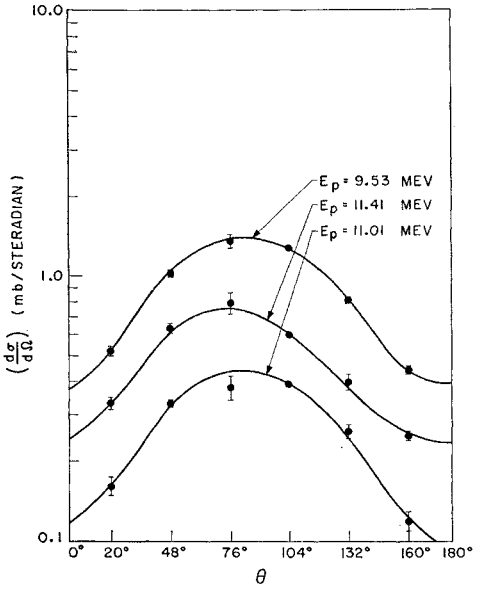

FIG. 28. Oxygen (e,pe') proton peak and valley angular distributions at $E_0=30$ MeV.

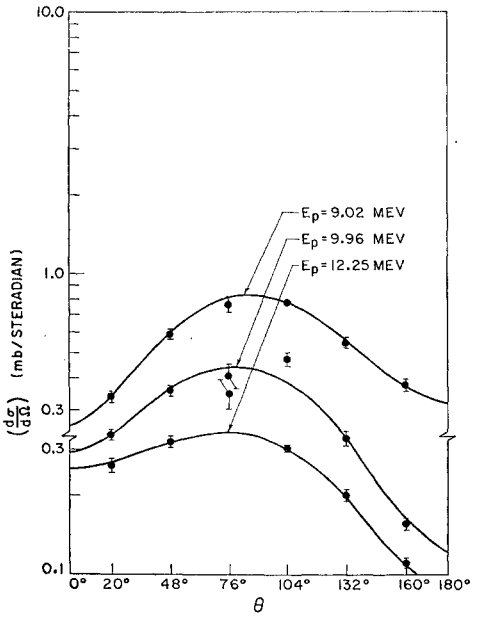

FIG. 29. Oxygen (e,pe') proton angular distributions at $E_0=30$ MeV.

(*b*) *Fluorine.* The F $d\sigma(\gamma,p)/d\Omega$ C'/A' values (Fig. 30) are ~ 0.5 for $E_p<7$ MeV, while for $E_p>7$ MeV they increase rapidly with E_p. The low values of C'/A' imply either a large component of a statistical emission process or a large proton relative angular momentum l. (According to the resonance direct theories $d\sigma/d\Omega\approx 1+\frac{1}{2}\sin^2\theta$ for large l.) The latter assumption would partially explain the low F^{19} $\int\sigma(\gamma,p)dE_\gamma$ because of the angular momentum barrier; but the (γ,n) yields would also be inhibited by this mechanism. According to the F^{19} $\sigma(\gamma,n)dE_\gamma$ measurements of Ferguson *et al.*,[43] this inhibition is not observed. Typical F $d\sigma(e,pe')/d\Omega$'s for $E_0=24.5$ MeV are shown in Fig. 31 with arbitrary ordinate units.

(*c*) *Neon.* The Ne $d\sigma(e,pe')/d\Omega$ exhibits the same

[65] C. Milone, S. Milone-Tamburino, R. Rinzivillo, A. Rubbino, and C. Tribuno, Nuovo cimento **7**, 729 (1958).
[66] P. Brix and E. R. Mascke, Z. Physik **155**, 109 (1959).
[67] E. D. Courant, Phys. Rev. **82**, 703 (1951).
[68] J. Eichler and H. A. Weidenmüller, Z. Physik **152**, 261 (1958).
[69] H E. Gove (private communication).
[70] D. Isabelle (private communication).
[71] G. E. Brown and L. S. Levinger, Proc. Phys. Soc. (London) **71**, 733 (1958).

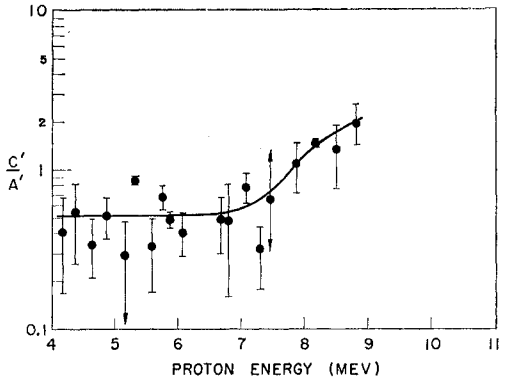

FIG. 30. Ratio of the even-parity terms in the angular distributions of the protons from F.

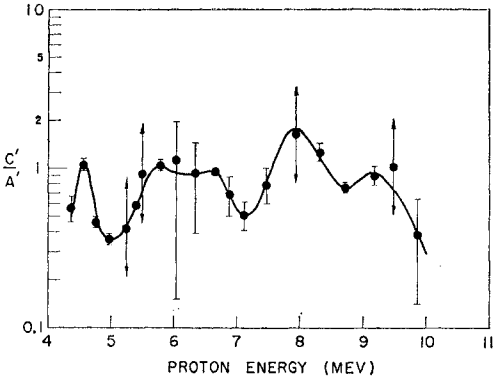

FIG. 32. Ratio of the even-parity terms in the angular distributions of the protons from Ne.

general behavior as O although C'/A' values (Fig. 32) are smaller—a significant fact since a resonant-state interaction with the valence nucleons which would produce a larger isotropic term than occurs in O seems unlikely in view of the sharper peaks in the Ne cross section. The similarity of shape of $d\sigma/d\Omega$ for the peak protons (which all have $C'/A' \approx 1$) is stressed in Fig. 33. The shift from backward to forward asymmetry on opposite sides of a peak, observed in O, is also seen for the second Ne peak in the $d\sigma/d\Omega$ of the 5.40- and 6.04-MeV protons in Fig. 34, along with the $d\sigma/d\Omega$ for the protons from the sides of other peaks. The angular distributions of Ne valley protons are shown in Fig. 35. According to the work of Komar and Iavor[45] the average value of C'/A' for $1 < E_p < 15$ MeV has increased to 2.5 for $E_{\gamma\max} = 80$ MeV. An upper limit for σ_{E2}/σ_{E1} is 3.6% from our work, although the average value is ~1%.

(*d*) *Carbon.* The C $d\sigma(\gamma,p)d\Omega$ has been measured by many experimenters for the direct reaction and by Gove *et al.*[59] for the inverse reaction. The agreement of the direct and inverse proton and photon angular distributions has been cited previously[56,59] as quantitative confirmation of detailed balance. Table VIII summarizes the existing data for the $C^{12}(\gamma,p_0)$ proton

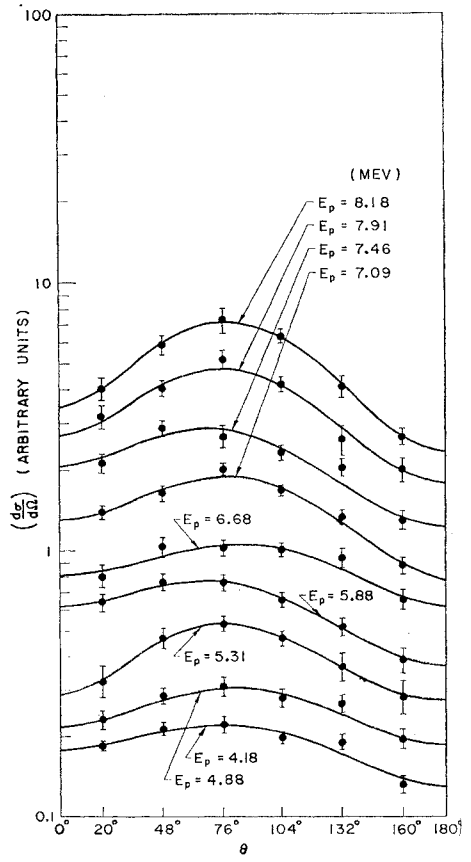

FIG. 31. Fluorine (*e,pe'*) proton angular distributions at $E_0 = 24.5$ MeV.

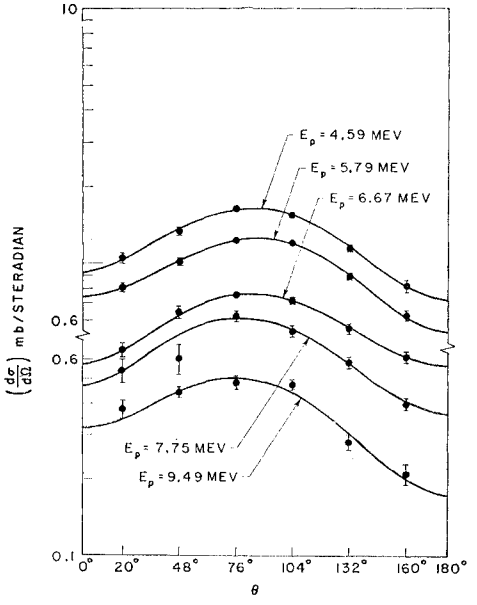

FIG. 33. Neon (*e,pe'*) proton peak angular distributions at $E_0 = 30$ MeV.

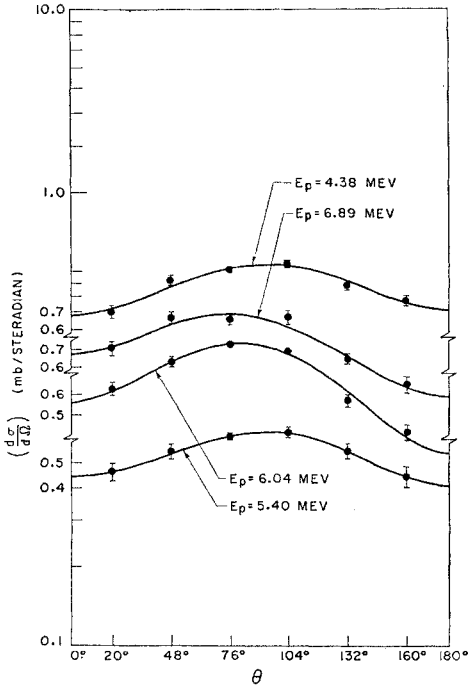

FIG. 34. Ne (e,pe') proton angular distributions from the low- and high-energy sides of the peaks at $E_0=30$ MeV.

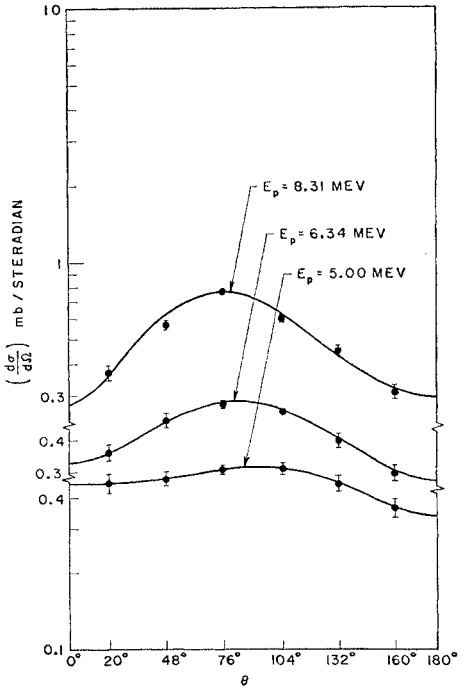

FIG. 35. Neon (e,pe') proton valley angular distributions at $E_0=30$ MeV.

and $B^{11}(p,\gamma_0)$ photon angular distributions. The C^{12} $d\sigma(e,pe')/d\Omega$ for $E_p<6.00$ MeV are shown in Fig. 36. Proton angular distributions from both sides of $\sigma_{\max}$ are shown in Fig. 37; the C'/A' values for C are plotted in Fig. 38. The resonance direct prediction with LS coupling is $C/A=\frac{3}{2}$.

(e) Aluminum. Al angular distributions are almost isotropic (Fig. 39). They have a slight forward asymmetry which suggests interference of states of opposite parity. The Al $d\sigma(\gamma,p)/d\Omega$ measurements of Hoffman and Cameron[72] at 30, 60, and 90° with $E_{\gamma\,\max}=25$ MeV suggest an isotropic angular distribution in agreement with our data. Our nearly isotropic angular distributions are in disagreement with the hypothesis of a relative $Al(\gamma,p)$ angular momentum of $l=3$ of Baglin *et al.*[63]

TABLE VIII. Comparison of the direct and inverse $C^{12}(\gamma,p)$ angular-distribution coefficients. The errors of this experiment are standard deviations.

Experiment	E_γ	C_0	C_1	C_2	C_3
$C^{12}(e,pe')$[a]	22–23	1	0.14±0.02	−0.50±0.03	···
$C^{12}(\gamma,p_0)$[b]	22.1	1±0.02	0.09±0.02	−0.56±0.04	−0.03±0.05
$B^{11}(p,\gamma_0)$[c]	22.5	1	0.12±0.03	−0.69±0.05	···
This experiment	22.4	1±0.05	0.16±0.09	−0.61±0.04	0.11±0.06

[a] See reference 56.
[b] See reference 57.
[c] See reference 59.

[72] M. M. Hoffman and A. G. W. Cameron, Phys. Rev. **92**, 1184 (1953).

IV. CONCLUSIONS

Our experiments provide information about the (e,pe') reaction, and as a consequence of the correspondence between electron and photon-induced reactions, about the (γ,p) reaction in O, F, Ne, C, Al, and to a lesser extent in Ar and B. This information is of sufficient

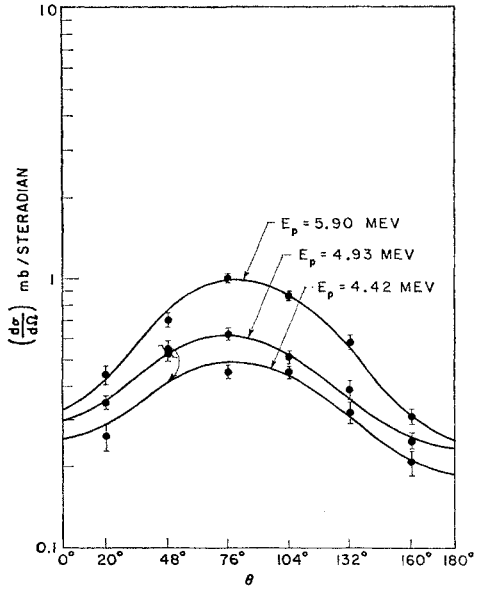

FIG. 36. Carbon (e,pe') proton angular distributions at $E_0=24.5$ MeV.

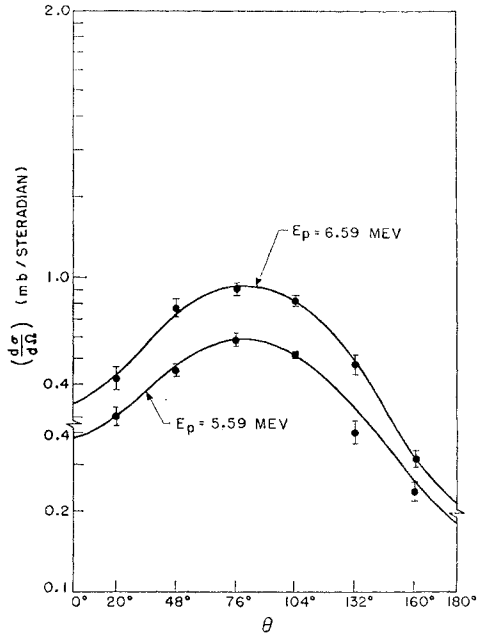

FIG. 37. Carbon (e,pe') proton angular distributions at $E_0=24.5$ MeV.

precision to motivate the expenditure of the considerable amount of theoretical labor which will be necessary to obtain quantitative understanding of our results. The following observations summarize the important implications of our work.

Our (e,pe') energy-distribution experiments have shown that gross structure of multiplicity greater than two does occur in the giant-resonance region in the (e,pe') reaction in O, F, and Ne. The occurrence of structure in F and Ne contradicts the predictions of the strong-correlation models of the photonuclear effect.[2,3] The quasi-agreement of the independent-particle model (IPM) calculations[7] with our O $\sigma(\gamma,p)$ and the mere occurrence of the structure in the F and Ne $\sigma(\gamma,p)$ are strong arguments for the validity of the independent-particle approach to the photonuclear effect in this region of Z. On the other hand, the $O(\gamma,p)$ IPM calculations of Elliot and Flowers,[7] while not comprehensive enough to predict all the structure in the O $\sigma(\gamma,p)$ (their calculations only semiquantitatively account for the location and relative $\int\sigma dE_\gamma$'s of the 9.5- and 11.5-MeV peaks), do not seem to predict the proper (γ,p) branching ratios to the 6.33-MeV (probably $\frac{3}{2}^-$) state and the ground $(\frac{1}{2}^-)$ state of N^{15}. Their branching-ratio prediction of 3.3 to 1 in favor of the $\frac{3}{2}^-$ state would imply that the region of the $O(\gamma,p)$ cross section from 20 to 26 MeV would contain an anomalously high 39% of the dipole sum-rule integrated cross-section prediction of 360 MeV-mb, compared with our value O^{16} $\int_{20}^{26}\sigma(\gamma,p)\times dE_\gamma$ of 32.4 MeV-mb. This serious and important discrepancy warrants further experimentation to determine the ratio of the ground to the excited states of N^{15} populated by the $O^{16}(\gamma,p)$ reaction for proton energies of less than 8 MeV.

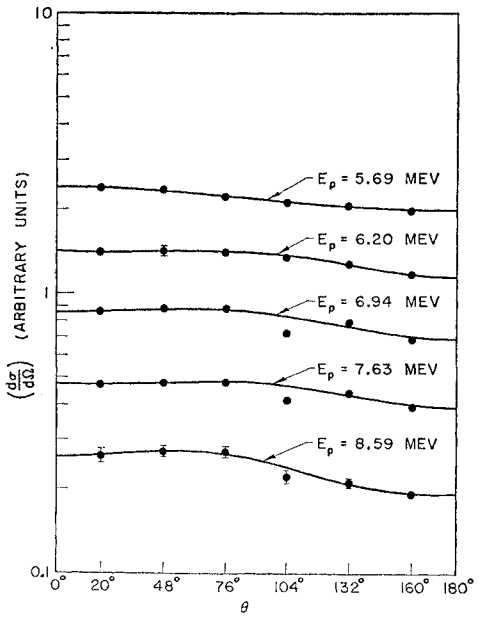

FIG. 39. Aluminum (e,pe') proton angular distributions $E_0=24.5$ MeV, $\Delta E_p\leq\pm0.25$ MeV.

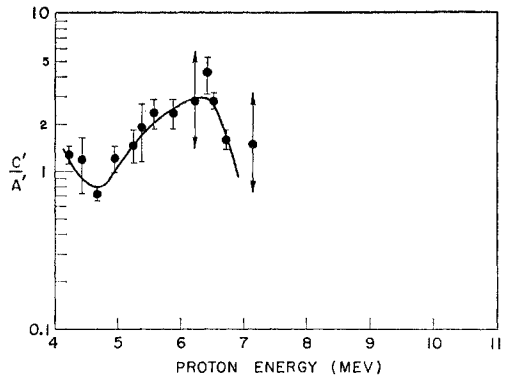

FIG. 38. Ratio of the even-parity terms in the angular distributions of protons from C.

As stated previously, detailed IPM calculations with which to compare our experimental results are not available; however, the following qualitative conclusions can be stated. Since one of the fundamental hypotheses of Wilkinson's IPM of the giant resonance is that the largest $E1$ contributions come from closed-shell transitions (transitions involving the O core in the case of F and Ne), the IPM predicts the giant-resonance proton-energy spectra of O, F, and Ne should be nearly the same; the presence of the F and Ne valence nucleons should merely broaden the peaks[8] observed in the O $\sigma(\gamma,p)$. In particular, since Ne has

only one more valence nucleon than F, their proton energy spectra should be nearly identical in the approximation that pairing forces or even-odd effects are unimportant. By the same reasoning the O, F, and Ne $d\sigma/d\Omega$'s should be similar. Experiment shows that none of these detailed IMP expectations are fulfilled. Thus, while the collective model's photonuclear predictions are not realized in this region of Z, the IPM predictions are not correct either. The occurrence of narrow resonances does seem to indicate, however, that the crude IPM wavefunctions should provide the better basis for a more accurate perturbation calculation of the photonuclear effect.

One additional remark may be made. Carbon O, and Ne are α-particle nuclei, and our experiments have shown that these nuclei have smaller giant-resonance "widths" than their non-α-particle neighbors, B and F. This condition seems to prevail in photonuclear reactions in heavier α-particle nuclei. Before extensive conjecture on this subject is made, more experiments are advisable. However, our angular distributions data provide an argument for O and Ne being more symmetric than F.

ACKNOWLEDGMENTS

The authors wish to acknowledge the important technical contributions to this work of William Ewings of the High-Energy Physics Laboratory Tube Shop, who skillfully fabricated the gas target cells, and of Edward Pathaway of the High-Energy Physics Laboratory Machine Shop. We thank W. K. H. Panofsky for his support of this work.